Final response for "Using ship-borne observations of methane isotopic ratio in the Arctic Ocean to understand methane sources in the Arctic"

Berchet Antoine[1,*], Isabelle Pison[1], Patrick M. Crill[2], Brett Thornton[2], Philippe Bousquet[1], Thibaud Thonat[1], Thomas Hocking[1], Joël Thanwerdas[1], Jean-Daniel Paris[1] and Marielle Saunois[1]

[1]Laboratoire des Sciences du Climat et de l'Environnement, CEA-CNRS-UVSQ, IPSL, Gif-sur-Yvette, France.
[2]Department of Geological Sciences, Stockholm University, SE-10691 Stockholm, Sweden.

Correspondence: A. Berchet (antoine.berchet@lsce.ipsl.fr)

1 Introductory replies

We thank the referees for their time and for giving fruitful comments and reviews to our manuscript. It helped improving our manuscript substantially. We address below their comments and implement corresponding corrections to the manuscript.

Comments from referee #1 and #2 are reported below in blue and red respectively. We include point-by-point replies and corresponding corrections to the manuscript are included between horizontal lines.

2 General comments

2.1 Method section and material description

1. **As much as I appreciate a concisely written paper, in this case the description of the methodology ended up being too short, so some characteristics of the optimization setup remain unclear. What exactly is optimized in this approach? In the setup, there are four different source types given for terrestrial areas, plus ESAS and boundary conditions (Table 1), and there are 24 regions differentiated (Figure 1). I assume that the authors optimized only wetland emissions from each terrestrial region, plus ESAS emissions and the 5 boundary conditions, which would make 30 free parameters to constrain (they discuss only 3 optimized parameters/source distributions in the results section ..). However, this is nowhere clearly documented, and given the available combinations of source types and regions, the total number could as well be 102. Also,the source of the starting values for the isotope ratio is given, but not the source of the uncertainty ranges. It may be the same, but this should be documented more clearly.**

   In general, I found the methodology could be clearer and some of the decisions in the data analysis approach could be justified (in some cases) and justified more thoroughly (in other cases). Without such additional information I would find it difficult to reproduce their results given their dataset.

In particular, in section 2.3, I would like to see the inversion approach described in more detail. It should be made completely clear what they are solving for in their state vector and which parameters go into the inversion. The approach of the inversion is also unclear to this reviewer. This could be rectified by detailing the inversion method, and then laying out the relevant equations (perhaps in the supplementary material).

We agree that the method section was detailed enough. We fully rewrote the corresponding section to allow the reader to fully understand what is done in our system. In particular, the equations linking the relative contributions of simulated sectors and regions and their isotopic signatures to the simulated isotopic ratio are given, as well as those describing the control vector and the inversion problem.

Below is the amended section:

To do so, δ^{13}C-CH_4 observations are implemented into a classical analytical Bayesian framework (Tarantola, 2005). The designed inversion system optimizes source signatures from different source types and different regions. At every time step when an isotopic observation is available, the system fits observations of isotopic ratios by altering the isotopic ratio in air masses coming from relevant source types and regions. Thus, the control vector contains one isotopic ratio value to optimize for each time step, each sector, and each region as detailed in Eq. 2 below.

The isotopic ratios of wetlands, solid fossil fuels, oil and gas, other anthropogenic sources from various land regions, and a potential variety of marine sources (gas field leaks, decomposing hydrates, degrading permafrost, etc.) from the East Siberian Arctic Shelf (ESAS), as well as from air masses coming from the sides and roof of our domain of simulations are optimized in the system. Apart from ESAS, emissions are spatially differentiated into 23 geographical regions (see Figure 1). Contributions from different regions and sectors are differentiated by computing so-called response functions by region, emission type and boundary side. That is to say, we carry out individual CHIMERE chemistry-transport simulations for every region, every type of emission and every side of the domain, all the other emissions and boundary conditions being switched off, resulting in an ensemble of 98 response functions (= 23 regions $\times$ 4 sectors + ESAS + 4 sides + top).

The simulated isotopic final composition $\mathbf{y}(t)$ at every given time step t when an observation is available is retrieved by scaling relative contributions according to assumed source signatures (or original average composition for boundary conditions) as follows:

$$\mathbf{y}(t) = \sum_{r \in \text{regions}} \sum_{s \in \text{sectors}} \alpha_{r,s}(t) \times \delta_{r,s}(t) \tag{1}$$

with r and s varying over all available regions and sectors respectively, $\alpha^t_{r,s}$ $(0 < \alpha^t_{r,s} < 1)$ the relative contribution of the sector s from region r at time t and $\delta^t_{r,s}$ the signature in ‰ of the sector s from region r at time t.

This linear relationship allows us to define the control vector $\mathbf{x}$ and the observation operator, linking the control vector to observations of isotopic ratios, to easily compute and scale the simulated isotopic composition:

$$\mathbf{y}(t) = \mathbf{H}(t)\mathbf{x}(t) \text{ with } \begin{cases} \mathbf{x}(t) &= \delta_{r,s}(t) \quad \forall (r,s) \in (\text{regions}) \times (\text{sectors}) \\ \mathbf{H}(t) &= (\alpha_{r,s}(t))_{r \in \text{regions}, s \in \text{sectors}} \end{cases} \tag{2}$$

Given the prior control vector $\mathbf{x}^{\text{b}}$ containing assumed source signatures before inversion, the observation vector $\mathbf{y}^{\text{o}}$ and the observation operator $\mathbf{H}$, optimized signatures are obtained by solving the Bayesian problem equation:

$$\mathbf{x}^{\text{a}} = \mathbf{x}^{\text{b}} + \mathbf{K}(\mathbf{y}^{\text{o}} - \mathbf{H}\mathbf{x}^{\text{b}}) \tag{3}$$

with $\mathbf{K} = \mathbf{P}^{\text{b}}\mathbf{H}^{\text{T}}(\mathbf{R} + \mathbf{H}\mathbf{P}^{\text{b}}\mathbf{H}^{\text{T}})^{-1}$ the Kalman matrix.

The matrix $\mathbf{R}$ represents uncertainties in the observations and in the capability of the model to reproduce them. In our case, we set them uniformly to $1.5‰$ ($1‰$ from observation errors and $0.5‰$ from simulation errors). The matrix $\mathbf{P}^{\text{b}}$ represents uncertainties and covariances in the prior knowledge we have on source signatures. We build the matrix $\mathbf{P}^{\text{b}}$ following the values in Tab. 1, deduced from Sherwood et al. (2017) and Sapart et al. (2017). Ranges and prior signatures for boundary conditions are deduced from global simulations with the model LMDZ. The temporal correlation is used to represent exponentially decreasing temporal correlation between the signature errors at two given times for the same sector and region.

As shown in Tab. 1, the values of source signatures are not well known and a very large range of signatures is available in the literature. To account for this large variety of realistic signatures, we carry out a Monte Carlo ensemble of 8000 inversions with varying prior signatures and uncertainties, instead of running one single inversion. Prior signatures are sample following a normal distribution with average and standard deviation from Tab. 1; the standard deviation is chosen as half of the min-max range. Uncertainties are sampled following a uniform distribution spanning over $[\sigma_{\text{ref}}/2, \sigma_{\text{ref}}]$, with σ_{ref} equals half of the min-max range of Tab. 1.

---

2. **In section 2.2, it sounds as though only OH is included as a sink, which ignores other potentially important sinks (such as the soil sink, Cl radical and stratospheric loss). Similarly, these sinks seemingly aren't accounted for in the optimisation, despite the fact that they also have larger uncertainties that vary in space and time. I am not suggesting the authors solve for them but they should at least acknowledge these other sinks for completeness. In section 2.2, it seems that only wetlands and anthropogenic emissions are used in the model, but again that is not clear from reading the manuscript. I suggest to address this explicitly in the main text or summarize the information in a table that lays out all the sources used in the model.**

We agree that our framework was not fully comprehensive in terms of both emissions and sinks processes. However, in order to keep the inversion framework simple, we did not include sources/sinks with negligible influence. We controled

that assumption using corresponding simulations. In terms of emissions, wild fires and in-land water systems play a significant role at the pan-Arctic scale, but once mixed and transported over long distances, corresponding simulated contributions are negligible (less than 2 ppb) in the region sampled during the SWERUS campaign. Similarly, the terrestrial soil sink is significant at the regional scale, but induce perturbations of less than 1 ppb at the sampling locations. The impact on isotopic ratios is below $0.02‰$ for all these processes.

Regarding the chlorine sink, we acknowledge that the very strong fractionation of the reaction with CH_4 may have a significant impact on concentrations and isotopic ratios. This sink occurs mainly in the upper stratosphere and in the Arctic Ocean boundary layer, The reaction in the stratosphere is included in the driving LMDZ simulations at the boundary conditions, and in the stratospheric part inside the domain, the residence time of air masses is too short to enable a significant impact. Regarding the chlorine sink in the boundary layer, when including the sink in our simulations, we saw an impact below 1 ppb and smaller that $0.01‰$ in the isotopic ratios.

We clarify all these aspects in the updated version of the manuscript:

CHIMERE runs use the following input data streams: (i) meteorological fields were downloaded from the European Centre for Medium Range Weather Forecasts (www.ecmwf.int) at 0.5° resolution every 3 hours; (ii) anthropogenic emissions were aggregated at the CHIMERE resolution from the EDGARv4.3.2 database at 0.1° horizontal resolution (Crippa et al., 2016); (iii) wetland emissions were interpolated from the model ORCHIDEE at 0.5° horizontal resolution (Ringeval et al., 2010); (iv) boundary CH_4 concentration fields were extracted from the general circulation model LMDZ; these global simulations include both the chemical sinks of OH and chlorine, as well as their impact on the isotopic ratios; (v) and isotopic signatures of the different sources were chosen from Sherwood et al. (2017).

The chemical sink by chlorine is not included in our set-up to keep simulations as light as possible. This sink can be separated into two main contributions: the upper stratosphere and the Arctic Ocean boundary layer. The upper stratosphere is not included in our model of simulation, but chlorine sink (and isotope fractionation) is expicitly accounted for in global LMDZ simulations used as boundary conditions for CHIMERE. Regarding the Arctic Ocean boundary layer, the set-up by Thonat et al. (2017) was adapted to our case, including boundary layer Cl sink using pre-computed fields from the model LMDZ-INCA. It resulted in differences of concentrations lower than 1 ppb over the Arctic ocean, and less than $0.02‰$ for the isotopic ratio of air masses, which is negligible compared to the signal we are inquiring into.

Other fluxes not included in our set-up play a significant role in the regional pan-Arctic budget, such as in-land water bodies, wild fires and the sink in soil, but have limited impact on our observations. These fluxes were tested in our case and were quantified to cause differences in simulated concentrations lower than 2 ppb, and less than $0.01‰$ in simulated isotopic ratios at the locations sampled during the SWERUS-C3 campaign.

2.2 Uncertainties and sensitivity

Building on this, it would be useful if the decisions that went into the setup were justified more clearly. For example, the authors describe that they assume emissions and atmospheric transport from the model are suitable due to how they match observations, but this is not rigorously tested. It might be possible to first solve for emissions and then for source signature (making a two-step inversion), or to perform sensitivity tests on their assumptions by, for example, perturbing model transport. Similarly, the lack of sinks other than OH, and the choice of which sources that are included, are not justified. The latter should be quite simple to rectify with a short explanation and some literature examples, or by laying out a table of the current understanding of methane source signatures.

This paper presents some evidence that the source signatures from wetlands is deviating between different Arctic terrestrial regions, but the accuracy of the results is not tested adequately. The authors provide a short statement that, given the good agreement between observations and simulations of total methane, they assume that the transport model is correct here (Section 2.3). Also, they provide fixed uncertainty ranges for prior isotope ratios, but fail to clearly document where these are coming from, and how trustworthy they are. The latter may be an easy fix, while the former is clearly reducing the impact of these results. I therefore request to add sensitivity studies where the role of transport and prior uncertainties on the outcome of the study is tested and quantified. It shouldn't be too much extra work to perturb the transport, and check if this results in major shifts in optimized isotope ratios for different regions. The same holds true for the assignment of prior uncertainties.

We thank the reviewers for pointing at this caveats in our work. We now give more details about the choices of the set-up in the Method section as explained above.

Regarding the uncertainties on our results, the original manuscript was indeed lacking a proper quantification of the robustness of our system outputs. We completed our work by doing a large ensemble of 8000 Monte-Carlo inversions with varying prior isotopic signatures and uncertainties of signatures. This allows us to include uncertainties properly. We do not explicitly include uncertainties in the transport, but they are included implicitly thanks to the $\mathbf{R}$ matrix, or observational matrix, which includes both instrument and transport errors. The posterior results are well within the instrument error, suggesting that further investigation on the model side are not necessary at this point (they may be necessary with new improved data sets with lower instrumental uncertainties).

Altogether, the ensemble of inversions points to similar conclusions, with a robust inclusion of uncertainties. Figure 3 and 4 were merged together for better clarity of the results.

Section 3.2 of the results was modified as follows:

Assuming that the mix of CH_4 sources is correct, we now attempt to separate hemispheric and regional contributions by optimizing source signatures for a set of geographical regions and different emission sectors in the Arctic as detailed in Sect. 2.3. Posterior isotopic ratios in Fig. 2 (bottom panel) follow most of the variability in observations, indicating the inverse method does fit the observations in a satisfying way. The rest of the signal is within the observation uncertainties of $0.1‰$. This proves

that even though the model is not perfect in representing the transport, it is reasonable to use simulated contributions to optimize isotopic signatures.

Figure 3 shows the posterior signature distributions as deduced from the 8000 Monte Carlo inversions for the four regions that are the most constrained by the observations, i.e. weighted by the sensitivity matrix as detailed in Sect. 2.3. Accounting for the sensitivity matrix, it appears that only the roof boundary conditions (i.e., air masses from the lower stratosphere), ESAS emissions (i.e., emissions from the Laptev, East Siberian, and Chukchi Seas) and wetland regions on the shores of the Arctic ocean are reasonably constrained by the SWERUS-C3 ship-based campaign. Even though anthropogenic emissions were optimized in our system, only the wetland emission sector is significantly constrained for land regions (Fig. 3). The lower stratosphere signatures span in a short range of $-48.5/-46.5‰$. Wetlands are suggested to have a heavier signature in Canada (optimal signature: $-69.9‰$) than in Eastern Siberia (optimal signature: $-65.9‰$, with a node of similar importance at $-55‰$), consistent with Ganesan et al. (2018) and the compilation by Thornton et al. (2016). Wetlands in Alaska exhibit a narrow posterior distribution at $-51.3‰$, with a secondary mode at $-75‰$. Alaska is thus well constrained by the inversion. However, the final value may suggest that the inversion has difficulties in differentiating collocated emissions and mixes the signal due to thermogenic sources with co-located wetland emissions, as it is the case in Alaska with extensive extraction of raw oil and gas.

Posterior ESAS signatures are significantly shifted by more than 5‰ to $-49.5‰$ from the prior signature towards lighter values. This compares with previous studies and points towards a mix of different processes taking place in the Arctic shelf such as inputs from the sea bed (James et al., 2016; Berchet et al., 2016; Skorokhod et al., 2016; Pankratova et al., 2018). The posterior signature could thus be explained by mixed biogenic and thermogenic sources, confirming that ESAS emissions, possibly including an hydrate contribution, are not as depleted as wetland sources (Cramer et al., 1999; Lorenson, 1999).

Overall, the approach developed here reveals that the spatial and temporal variations of isotopic source signatures must be accounted for in order to properly represent δ^{13}C-CH_4 observations. Such an approach does not allow us to reach definitive conclusions when considering the spread of the inferred regional isotopic signatures. However, it is crucial to account for isotopic ratios to avoid misallocating methane flux variations in methane inversions. We also show that atmospheric δ^{13}C-CH_4 signals can be significant (larger than observation errors), indicating a good potential for the use of isotopic observations based on oceanic campaign to improve our knowledge of the Arctic methane cycle. Finally, the weight of the boundary conditions in the signal points at necessary progress in global simulations (including fractionating chemical reactions in the stratosphere) of CH_4 atmospheric isotopic ratios.

---

3 Technical comments

1. **The introduction could be strengthened by additional material on existing attempts to constrain Arctic CH4 sources in different regions, with different approaches. Where does the controversy on ESAS emissions stem**

from, and where are the knowledge gaps? How exactly will this campaign contribute to filling these gaps?

We added references and explanation about the ESAS controversy in the introduction following the referee's recommendation

---

Moreover, in addition to increased CH_4 emissions from wetlands and thawing permafrost, increasing ocean temperatures could lead to the destabilization of methane clathrates on the Arctic continental shelf, potentially emitting large quantities of CH_4 . For instance, significant point emissions have been detected along the East Siberian Arctic Shelf (Shakhova et al., 2010) taking the shape of CH_4 flaring from the sea floor extending up to the surface. However, upscaling point measurements of hot spots proves difficult and there is no proof that such methane hydrate emissions are currently reaching the atmosphere in large quantities (Berchet et al., 2016; Pisso et al., 2016; Ruppel and Kessler, 2017). Other potential Arctic seafloor sources of CH_4 include emissions from degrading subsea permafrost (Dmitrenko et al., 2011), leakage from natural gas reservoirs, and degrading terrestrial organic carbon transported onto the continental shelf (Charkin et al., 2011).

---

2. **As mentioned above, the Methods section is very short, sometimes too short. For the interested reader more details on the methodology (e.g. on the CHIMERE model) should be provided either in an appendix, or in an SI section. In Section 3.3, more details on the optimization target and strategy need to be provided also in the main text (see details above).**

We fully agree with this point, which was fixed following general comments above.

3. **Figure 2 raises the question why the cumulative contributions of top and 4x side components are so stable over time, given the pronounced variability in contributions from different sides of the model domain, which is also discussed in Section 3.1? Maybe it would be helpful to show the mean concentrations from the global model that were taken as a reference for the 5 boundary values applied here.**

The stable contribution by boundary conditions is an optical illusion. There is a change in the y-axis at 1800 ppb making it look like the total of boundary conditions is flat, while it is not the case. There is a stretching by a factor 4 above and below 1800 ppb on the figure. The limit has been shifted to 1700 ppb to highlight the change in total boundary contribution and the legend has be amended accordingly.

As suggested by the reviewer, we also include an additional panel with the total simulations and observations only.

The legend reads as follows now:

(top panel) Observed and simulated total CH_4 concentrations; (middle panel) simulated contributions to total CH_4 concentrations; individual regions simulated by the model (see Fig. 1) are aggregated into two main continental components: North-America (NA) and Eurasia; light green areas depict Eurasian (mostly Siberian) wetlands, while dark green ones are North American wetlands. Shaded blue areas represent contributions from the sides of the CHIMERE simulation domain (see Fig. 1); orange shades represent minor anthropogenic contribution. So-called "top" line gives the simulated concentrations originating from the lower stratosphere (i.e., from the top of CHIMERE simulation domain). Please note the gap in y-axis scale at 1700 ppb highlighted by the dash line. (bottom panel) Observed and simulated isotopic ratios before (prior) and after (posterior) inversion.

---

4. **One confusing part of Section 3.2 is the mentioning of 'temporal variability' - what are the authors referring to? Obviously, there was no temporal variability in the source isotope ratios detected, or at least none is shown (or discussed) in any of the results. The only temporal variability shown is that of the retrieved isotope signal in the SWERUS data (Figure 2, bottom), but here the variability has been largely attributed to shifts in the origin of air masses, and accordingly source regions. The statement on temporal variability is repeated also in the conclusions. Please clarify.**

We agree that due to the unclear method parts, the mentioning of 'temporal variability' was misleading. We optimize the isotopic ratios of each contributions in the air masses sampled by SWERUS. Thus, for every time stamp of observation, posterior signatures are available. To keep consistent variability for each sector/region, temporal correlations were included as detailed in Table 1 and Eq.2-3.

The relevant amended part of the Method section are repeated below. We hope such clarifications will help the reader follow our approach easily.

In the end, we obtain hourly posterior signatures for each simulated sector and region for each of the 8000 inversions. Even though posterior signatures are available for each region and each sector at each observation time step, we do not inquire into the temporal variability of sources as constraints provided by the SWERUS observations are very heterogeneous in time and space. Instead, we compute overall posterior distributions for each simulated sector and region based on an ensemble of 8000000 (=8000 inversions $\times$ 1000 hourly observations). To minimizing the impact of control vector components that are ill-constrained by the inversion, all data points are not evenly counted in posterior distributions. Posterior distributions of signatures are computed accounting for all the Monte Carlo samples and weighted by the corresponding values of the sensitivity matrix $\mathbf{KH}$ (Cardinali et al., 2004), which gives an indicator of how much observations constrain one component of the control vector. The posterior optimal signature for each region and sector is computed as the maximum of the probability distribution.

---

5. **Finally, please make sure your reference list is up-to-date (old discussion papers cited)**

   We updated papers that were still cited as discussion papers while accepted long ago. We try including the most recent publications on methane in the Arctic. We apologize for any missing reference not come to our knowledge.

6. **Some minor corrections include spelling and grammar errors. Some sentences do not make sense, e.g. the first sentence in the abstract. In addition, some further details of the how the model works could go into the supplementary information section. Figure 2 could be made clearer – it's a little hard to discern the observation line from the model results in the top panel. Maybe a separate panel with total model and observations would solve this. Also, the introduction would be stronger if it laid out current understanding of Arctic methane source types, thereby justifying the article by highlighting our current lack of understanding.**

   We thoroughly spellcheck and proof-read the updated version of the manuscript to provide an English writing as good as possible. Figure 2 was made clearer as detailed above. We added references in the introduction to better set the scene.

References

Berchet, A., Bousquet, P., Pison, I., Locatelli, R., Chevallier, F., Paris, J.-D., Dlugokencky, E. J., Laurila, T., Hatakka, J., Viisanen, Y., Worthy, D. E. J., Nisbet, E., Fisher, R., France, J., Lowry, D., Ivakhov, V., and Hermansen, O.: Atmospheric constraints on the methane emissions from the East Siberian Shelf, Atmos. Chem. Phys., 16, 4147–4157, https://doi.org/10.5194/acp-16-4147-2016, http://www.atmos-chem-phys.net/16/4147/2016/, 2016.

Cardinali, C., Pezzulli, S., and Andersson, E.: Influence-matrix diagnostic of a data assimilation system, Q. J. R. Meteorol. Soc., 130, 2767–2786, https://doi.org/10.1256/qj.03.205, http://onlinelibrary.wiley.com/doi/10.1256/qj.03.205/abstract, 2004.

Charkin, A. N., Dudarev, O. V., Semiletov, I. P., Kruhmalev, A. V., Vonk, J. E., S\'anchez-Garc\'ia, L., Karlsson, E., and Gustafsson, \.: Seasonal and interannual variability of sedimentation and organic matter distribution in the Buor-Khaya Gulf: the primary recipient of input from Lena River and coastal erosion in the southeast Laptev Sea, Biogeosciences, 8, 2581–2594, https://doi.org/https://doi.org/10.5194/bg-8-2581-2011, https://www.biogeosciences.net/8/2581/2011/bg-8-2581-2011.html, 2011.

Cramer, B., Poelchau, H. S., Gerling, P., Lopatin, N. V., and Littke, R.: Methane released from groundwater: the source of natural gas accumulations in northern West Siberia, Marine and Petroleum Geology, 16, 225–244, https://doi.org/10.1016/S0264-8172(98)00085-3, http://www.sciencedirect.com/science/article/pii/S0264817298000853, 1999.

Crippa, M., Janssens-Maenhout, G., Dentener, F., Guizzardi, D., Sindelarova, K., Muntean, M., Van Dingenen, R., and Granier, C.: Forty years of improvements in European air quality: regional policy-industry interactions with global impacts, Atmospheric Chemistry and Physics, 16, 3825–3841, https://doi.org/https://doi.org/10.5194/acp-16-3825-2016, https://www.atmos-chem-phys.net/16/3825/2016/, 2016.

Dmitrenko, I. A., Kirillov, S. A., Tremblay, L. B., Kassens, H., Anisimov, O. A., Lavrov, S. A., Razumov, S. O., and Grigoriev, M. N.: Recent changes in shelf hydrography in the Siberian Arctic: Potential for subsea permafrost instability, Journal of Geophysical Research: Oceans, 116, https://doi.org/10.1029/2011JC007218, https://agupubs.onlinelibrary.wiley.com/doi/10.1029/2011JC007218, 2011.

Ganesan, A. L., Stell, A. C., Gedney, N., Comyn-Platt, E., Hayman, G., Rigby, M., Poulter, B., and Hornibrook, E. R. C.: Spatially Resolved Isotopic Source Signatures of Wetland Methane Emissions, Geophysical Research Letters, 45, 3737–3745, https://doi.org/10.1002/2018GL077536, https://agupubs.onlinelibrary.wiley.com/doi/abs/10.1002/2018GL077536, 2018.

James, R. H., Bousquet, P., Bussmann, I., Haeckel, M., Kipfer, R., Leifer, I., Niemann, H., Ostrovsky, I., Piskozub, J., Rehder, G., Treude, T., Vielstädte, L., and Greinert, J.: Effects of climate change on methane emissions from seafloor sediments in the Arctic Ocean: A review, Limnology and Oceanography, 61, S283–S299, https://doi.org/10.1002/lno.10307, https://aslopubs.onlinelibrary.wiley.com/doi/abs/10.1002/lno.10307, 2016.

Lorenson, T.: Gas composition and isotopic geochemistry of cuttings, core, and gas hydrate from the JAPEX/JNOC/GSC Mallik 2L-38 gas hydrate research well, Bulletin of the Geological Survey of Canada, p. 21, http://pubs.er.usgs.gov/publication/70021662, 1999.

Pankratova, N., Skorokhod, A., Belikov, I., Elansky, N., Rakitin, V., Shtabkin, Y., and Berezina, E.: EVIDENCE OF ATMOSPHERIC RESPONSE TO METHANE EMISSIONS FROM THE EAST SIBERIAN ARCTIC SHELF, https://ges.rgo.ru/jour/article/view/383, 2018.

Pisso, I., Myhre, C. L., Platt, S. M., Eckhardt, S., Hermansen, O., Schmidbauer, N., Mienert, J., Vadakkepuliyambatta, S., Bauguitte, S., Pitt, J., Allen, G., Bower, K. N., O'Shea, S., Gallagher, M. W., Percival, C. J., Pyle, J., Cain, M., and Stohl, A.: Constraints on oceanic methane emissions west of Svalbard from atmospheric in situ measurements and Lagrangian transport modeling, J. Geophys. Res. Atmos., 121, 2016JD025 590, https://doi.org/10.1002/2016JD025590, http://onlinelibrary.wiley.com/doi/10.1002/2016JD025590/abstract, 2016.

Ringeval, B., de Noblet-Ducoudré, N., Ciais, P., Bousquet, P., Prigent, C., Papa, F., and Rossow, W. B.: An attempt to quantify the impact of changes in wetland extent on methane emissions on the seasonal and interannual time scales, Global Biogeochemical Cycles, 24, https://doi.org/10.1029/2008GB003354, http://onlinelibrary.wiley.com.biblioplanets.gate.inist.fr/doi/10.1029/2008GB003354/abstract, 2010.

Ruppel, C. D. and Kessler, J. D.: The interaction of climate change and methane hydrates, Reviews of Geophysics, 55, 126–168, https://doi.org/10.1002/2016RG000534, https://agupubs.onlinelibrary.wiley.com/doi/10.1002/2016RG000534, 2017.

Sapart, C. J., Shakhova, N., Semiletov, I., Jansen, J., Szidat, S., Kosmach, D., Dudarev, O., Veen, C. v. d., Egger, M., Sergienko, V., Salyuk, A., Tumskoy, V., Tison, J.-L., and Röckmann, T.: The origin of methane in the East Siberian Arctic Shelf unraveled with triple isotope analysis, Biogeosciences, 14, 2283–2292, https://doi.org/https://doi.org/10.5194/bg-14-2283-2017, https://www.biogeosciences.net/14/2283/2017/, 2017.

Shakhova, N., Semiletov, I., Salyuk, A., Yusupov, V., Kosmach, D., and Gustafsson, O.: Extensive Methane Venting to the Atmosphere from Sediments of the East Siberian Arctic Shelf, Science, 327, 1246–1250, https://doi.org/10.1126/science.1182221, http://www.sciencemag.org/content/327/5970/1246, 2010.

Sherwood, O. A., Schwietzke, S., Arling, V. A., and Etiope, G.: Global Inventory of Gas Geochemistry Data from Fossil Fuel, Microbial and Burning Sources, version 2017, Earth System Science Data, 9, 639–656, https://doi.org/https://doi.org/10.5194/essd-9-639-2017, https://www.earth-syst-sci-data.net/9/639/2017/, 2017.

Skorokhod, A. I., Pankratova, N. V., Belikov, I. B., Thompson, R. L., Novigatsky, A. N., and Golitsyn, G. S.: Observations of atmospheric methane and its stable isotope ratio (δ^{13}C) over the Russian Arctic seas from ship cruises in the summer and autumn of 2015, Dokl. Earth Sc., 470, 1081–1085, https://doi.org/10.1134/S1028334X16100160, https://doi.org/10.1134/S1028334X16100160, 2016.

Tarantola, A.: Inverse problem theory and methods for model parameter estimation: SIAM, Society for Industrial and Applied Mathematics, 3600, 19 104–2688, 2005.

Thonat, T., Saunois, M., Bousquet, P., Pison, I., Tan, Z., Zhuang, Q., Crill, P. M., Thornton, B. F., Bastviken, D., Dlugokencky, E. J., Zimov, N., Laurila, T., Hatakka, J., Hermansen, O., and Worthy, D. E. J.: Detectability of Arctic methane sources at six sites performing continuous atmospheric measurements, Atmos. Chem. Phys., 17, 8371–8394, https://doi.org/10.5194/acp-17-8371-2017, https://www.atmos-chem-phys.net/17/8371/2017/, 2017.

Thornton, B. F., Wik, M., and Crill, P. M.: Double-counting challenges the accuracy of high-latitude methane inventories, Geophys. Res. Lett., p. 2016GL071772, https://doi.org/10.1002/2016GL071772, http://onlinelibrary.wiley.com/doi/10.1002/2016GL071772/abstract, 2016.

Using ship-borne observations of methane isotopic ratio in the Arctic Ocean to understand methane sources in the Arctic

Berchet Antoine[1,*], Isabelle Pison[1], Patrick M. Crill[2], Brett Thornton[2], Philippe Bousquet[1], Thibaud Thonat[1], Thomas Hocking[1], Joël Thanwerdas[1], Jean-Daniel Paris[1] and Marielle Saunois[1]

[1]Laboratoire des Sciences du Climat et de l'Environnement, CEA-CNRS-UVSQ, IPSL, Gif-sur-Yvette, France.
[2]Department of Geological Sciences, Stockholm University, SE-10691 Stockholm, Sweden.

Correspondence: A. Berchet (antoine.berchet@lsce.ipsl.fr)

Abstract.

~~The large variety and heterogeneity of sources in remote areas in the Arctic are hard to document, which makes the Arctic regional methane budget very uncertain. In situ~~ Characterizing methane sources in the Arctic remains challenging, due to the remoteness, heterogeneity, and variety of such emissions. *In situ* campaigns provide valuable data sets to reduce these uncertainties. Here we analyse data from the ~~SWERUS-C3 campaign, on-board the icebreaker *Oden*, that took place during~~ summer 2014 ~~in the Arctic Ocean along the Northern Siberian and Alaskan shores~~SWERUS-C3 campaign in the eastern Arctic Ocean, offshore Siberia and Alaska. Total concentrations of methane, as well as ~~isotopic ratios~~ relative concentrations of $^{12}CH_4$ and $^{13}CH_4$ were measured continuously during this campaign for 35 days in July and August~~2014.~~. Using a chemistry-transport model, we link observed concentrations and isotopic ratios to regional emissions and hemispheric transport structures. A simple inversion system helped ~~constraining~~ constrain source signatures from wetlands in Siberia and Alaska, and oceanic sources, as well as the isotopic composition of lower stratosphere air masses. The variation in the signature of low stratosphere air masses, due to strongly fractionating chemical reactions in the stratosphere, was suggested to explain a large share of the observed variability in isotopic ratios. These ~~points at required~~ results point at necessary efforts to better simulate large scale transport and chemistry patterns to ~~use~~ make a relevant use of isotopic data in remote areas. It is also found that constant and homogeneous source signatures for each type of emission in ~~the~~ a given region (mostly wetlands, and oil and gas industry ~~)~~ ~~is~~ in our case at high latitudes) are not compatible with the strong synoptic isotopic signal observed in the Arctic. A regional gradient in source signatures is highlighted between Siberian and Alaskan wetlands, the ~~later ones having a lighter signatures than the first ones.~~ latter having lighter signatures (more depleted in ^{13}C). Finally, our results suggest that marine emissions of methane from Arctic continental shelf sources are ~~suggested to be a mixture of methanefrom a dominant thermogenic origin and~~ dominated by thermogenic-origin methane, with a secondary biogenic ~~one, consistent with previous in-situ isotopic analysis of seepage along the Siberian shores~~source as well.

1 Introduction

Methane (CH_4) is both a potent greenhouse gas and a precursor of ozone with very diverse sources and sinks in the atmosphere (Saunois et al., 2016). ~~About 60% (in mass) of CH_4 emissions to the atmosphere are due to microbial activity in anaerobic environments: mainly natural wetlands, managed wetlands (such as rice paddies), landfills, waste-water facilities and the intestines of ruminants (domestic and wild) and termites. CH_4 is also emitted through fossil fuel leakages during extraction, transport and distribution. Finally, CH_4 is emitted by biomass burning (wildfires, agricultural fires and biofuels). The~~ The wide variety of CH_4 sources and their spatial and temporal heterogeneity make the uncertainties on CH_4 budgets very large, ~~from the regional to the~~ on both regional and global scales (Saunois et al., 2016). ~~They impair~~ This impairs our understanding of the variations of atmospheric concentrations, particularly of which sources of methane and/or regions are causing these variations, which have been ~~fast in the last~~ rapid in recent decades (Dlugokencky et al., 2009; Nisbet et al., 2016; Saunois et al., 2017; Nisbet et al., 2019; Turner et al., 2019).

In the Arctic, major CH_4 sources are natural wetlands, in-land waters (lakes, streams, deltas, estuaries), leaks from oil and gas extraction and transport, wildfires, seabed and geological seepage. The magnitude of all these sources suffers with very high uncertainties ~~(McGuire et al., 2009; Kirschke et al., 2013; Arora et al., 2015; Berchet et al., 2016)~~ (McGuire et al., 2009; Kirschke et al., 2013; Berchet et al., 2015; Arora et al., 2015; Berchet et al., 2016; Ishizawa et al., 2019) . The large areas of wetlands above 50°N and the high sensitivity of their CH_4 emissions to the changing climate make this zone a ~~key-region~~ key region for the global CH_4 budget. The present uncertainties on CH_4 sources and sinks in the Arctic are very large, due to the complexity of the involved processes and the difficult access to these remote regions (e.g., Thornton et al., 2016b; Bohn et al., 2015). Moreover, in addition to increased CH_4 emissions from wetlands and thawing permafrost, increasing ocean temperatures could lead to the destabilization of methane ~~clathrates~~ hydrates on the Arctic continental shelf, potentially emitting large quantities of CH_4 ~~, though~~ . For instance, significant point emissions have been detected along the East Siberian Arctic Shelf (Shakhova et al., 2010, 2014; Thornton et al., 2016a, 2020) taking the shape of CH_4 flaring from the sea floor extending up to the surface. However, upscaling point measurements of "hot spots" proves difficult and there is no proof that such methane hydrate emissions are currently reaching the atmosphere in large quantities ~~(Ruppel and Kessler, 2017)~~ (Berchet et al., 2016; Pisso et al., 2016; Ruppel and Kessler, 2017). Other potential Arctic seafloor sources of CH_4 include emissions from degrading subsea permafrost (Dmitrenko et al., 2011), leakage from natural gas reservoirs, and degrading terrestrial organic carbon transported onto the continental shelf (Charkin et al., 2011). CH_4 emissions from the Arctic would then have a positive feedback on climate change. ~~Yet, The potential magnitude and timing of future methane emissions from the Arctic remain unsatisfactorily constrained.~~ A better knowledge of Arctic CH_4 emissions would reduce uncertainties in its global budget, and help to better quantify the sensitivity of Arctic regional sources and sinks to climate change.

~~The current generation of satellites observing CH_4 with passive methods in the Short-Wave-InfraRed (SWIR) proves helpless in providing a good coverage of Arctic regions, due to cloud, ice and snow cover, as well as the Arctic night (Xiong et al., 2008) . The Merlin mission equipped with an active LIDAR is to be launched in 2024 and may radically improve the data coverage of CH_4 in the Arctic. For the time being and the next years, the monitoring of the Arctic atmosphere relies on in situ measurements.~~

For more than ten years, atmospheric measurements of methane concentrations have been performed in the Arctic, either at surface stations (e.g., Arshinov et al., 2009; Sasakawa et al., 2010; Dlugokencky et al., 2014), during mobile field campaigns such as the YAK-AEROSIB aircraft campaigns (Paris et al., 2010) and the TROICA train campaign (Tarasova et al., 2006, 2009) or during oceanographic campaigns (e.g., Pisso et al., 2016; Yu et al., 2015; Pankratova et al., 2019). In the present work, we analyze data from the SWERUS-C3 campaign on-board a ship in the Arctic Ocean during summer 2014 (Thornton et al., 2016a). Such short-term mobile campaigns are necessary to complement the limited number of long-term fixed, mostly coastal stations currently available. In particular, oceanic campaigns are expected to provide information on oceanic sources but also on land sources located upwind. However, CH_4 from various sources is being mixed during the atmospheric transport of the air masses, which makes it difficult to separate them without resorting to numerical modelling (Berchet et al., 2016).

Atmospheric inversions merge together observations, numerical modelling and emission data sets to attribute the observed variability in CH_4 concentrations to emitting regions and thus optimize the CH_4 budget. Such methods were successfully applied in the Arctic using ~~in situ fixed stations (e.g., ?Thompson et al., 2017)~~*in situ* fixed stations (e.g., Berchet et al., 2015; Thompson et al , as well as satellites when available (Tan et al., 2016). But despite technical progress in numerical modelling and inversion methods, it is hardly feasible to separate co-located emissions from different emitting sectors upwind observation sites based on ~~CH_4 observations only~~observations of CH_4 concentrations alone. Observations of methane isotopic ratios could help separating emission sectors as the main emission processes are isotopically fractionating, causing significantly different isotopic source signatures. For example, high-latitude wetlands were attributed signatures in a range of ~~-80/ -55‰~~ -80 to -55‰ (Thornton et al., 2016b; Fisher et al., 2017; Ganesan et al., 2018). The δ^{13}C-CH_4 signature of atmospheric CH_4 above the Arctic Ocean has been previously reported in the range of ~~-50/ -47‰~~ -50 to -47‰ (Yu et al., 2015; Pankratova et al., 2019). Isotopes have already been used to characterise the origin of air masses in the Arctic (Fisher et al., 2011; Warwick et al., 2016)~~and~~ , though these studies concluded that refinements in qualifying source emission isotopic signatures are required. ~~In particular, in situ measurements of source signatures are being made in various environments but their strong variabilities make any upscaling difficult, pointing at the necessity of integrated information on emission signatures.~~

In the following, we explore the potential of using observations of isotopic ratios in the Arctic Ocean together with total CH_4 concentrations to separate ~~emission sources around the Arctic Circle~~pan-Arctic emission sources. We further analyse emission isotopic signatures in the Arctic from integrated atmospheric observations. We base our analysis on the unique observation set collected during the ship-based campaign SWERUS-C3 during summer 2014 in the Arctic Ocean. By comparing measurements to simulations of total CH_4 and isotopic ratio, we analyse to what extent the observable signal in the Arctic Ocean is exploitable in a numerical inversion system. In Sect. 2, we explain our inversion approach alongside giving details on the SWERUS-C3 observation campaign and on the model CHIMERE used in our study. In Sect. 3, we compare observations to simulations to assess the main contributions to the signal variability, and then implement a simplified inversion system to quantify isotopic emission signatures from various emission sectors around the Arctic.

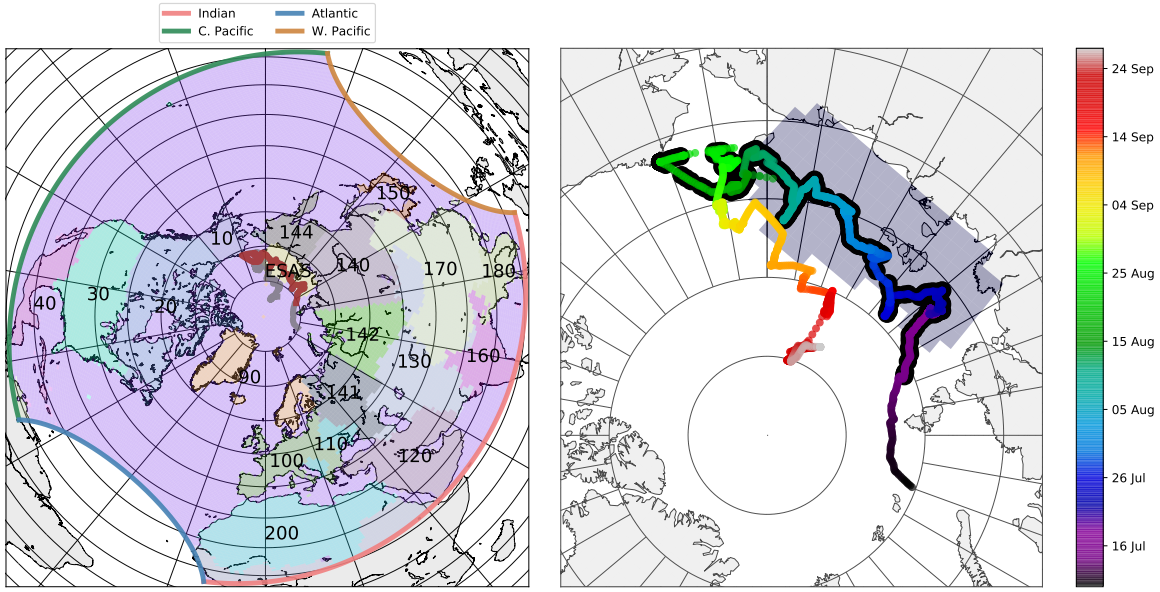

Figure 1. Path of the icebreaker *Oden* during the SWERUS-C3 campaign and domain of simulations. (left) The ship positions are represented by gray and brown dots, with brown points corresponding to locations where isotopic observations where carried out. The area delimited by coloured lines is the domain of CHIMERE simulations used for this study (see Sect. 2.2). The shaded areas and associated numbers correspond to the regions and their IDs used to separate contributions from remote emissions to the observed signal, as detailed in Sect. 2.3. ESAS = East Siberian Arctic Shelf. CHIMERE boundary conditions are split along the four sides of the domain as indicated by the coloured lines. (right) Zoom on the area covered by the campaign. The icebreaker's locations are coloured depending on their corresponding dates. Ship positions with a black edge are locations where isotopic observations where carried out. More details on the campaign in Thornton et al. (2016a). The shaded area corresponds to the ESAS emission region used in our simulation set up.

2 Methods

2.1 Campaign and instrument description

Observations were carried out during the SWERUS-C3 campaign onboard the Swedish icebreaker *Oden* between July 14th and September 26th, 2014. The cruise path was ~~thru~~ throught the central and outer Laptev and East Siberian seas, and finally the Chukchi Sea to Point Barrow, Alaska, in a first leg (see Fig. 1). A second leg of the cruise headed north from Point Barrow back through the Chukchi Sea and into the Arctic Ocean~~; atmospheric CH_4 observations continued until September~~ . As shown in Fig. S1 in supplementary materials, sea ice cover was present during a large portion of the campaign. Regions known to have active seafloor gas seeps (see Thornton et al., 2016a) occurred in both ice-free (in the Laptev Sea) and ice-covered (in the East Siberian Sea) regions.

Concentrations of total CH_4 were measured during the whole campaign using an off-axis cavity ring-down laser spectrometer, from Los Gatos Research (LGR) Inc. (Model 0010, FGGA 24EP, Mountain View, California, USA). Air inlets were located

at 9, 15, 20, and 35 m above the sea surface; air was pulled through all inlets continuously, and analyzed from one inlet at a time for 2 minutes before switching to the next inlet. Data ~~was~~ were filtered using wind speed and direction to avoid contamination from the ship exhaust. As no local sources influenced our measurements, concentrations are similar at all levels. We concatenate measurements from all inlets indifferently for our study. The spectrometer was calibrated every two hours using ~~a~~ two synthetic air target gases; the target gases themselves were calibrated before, during, and after the cruise to ~~a~~ two NOAA Earth System Research Laboratory certified ~~standard~~ standards for CH_4 . The reported precision was 0.5 ppb. Further details on the campaign conditions and instrument configuration are available in Thornton et al. (2016a).

Isotopic ratios were measured only during the first leg of the campaign, from July 14th to August 26th (see Fig. 1) using an Aerodyne Research, Inc (Billerica, MA, USA) direct absorption interband cascade laser spectrometer. This spectrometer measured the concentrations of the CH_4 isotopologues $^{12}CH_4$, $^{13}CH_4$, and CH_3D, the latter of which is not discussed in the current paper. The more common isotope ratio mass spectrometry methods directly provide (as their name implies) an isotope ratio. In contrast, because the Aerodyne spectrometer measures the individual isotopologues, they must be individually calibrated before converting to δ^{13}C-CH_4 values; this method is described in McCalley et al. (2014).

2.2 Model description

The Eulerian model CHIMERE (Menut et al., 2013) was run to simulate total concentrations of CH_4 as well as partial $^{12}CH_4$ and $^{13}CH_4$ concentrations to compute CH_4 isotopic ratios afterwards using the following formula:

$$\delta^{13}C = \frac{\left(\frac{[^{13}C]}{[^{12}C]}\right)_{sim}}{\left(\frac{[^{13}C]}{[^{12}C]}\right)_{ref}} - 1 \quad (1)$$

with $\left(\frac{[^{13}C]}{[^{12}C]}\right)_{ref} = 0.0112372$ the reference ratio from Craig (1957).

The domain of simulations spans over most of the ~~North~~ Northern hemisphere with a horizontal resolution of ~ 100 km in order to include most contributions from distant sources (see Fig. 1). Similarly, the model uses 34 vertical levels from the surface up to 150 hPa to represent stratosphere-to-troposphere intrusions. A spin-up period of six months prior to the campaign was used to properly assess the impact of air masses transported for long periods before reaching the Arctic ocean. The chemical sink of CH_4 by OH radicals is explicitly computed in CHIMERE using pre-computed fixed OH fields from the chemical model LMDZ-INCA (Hauglustaine et al., 2004; Folberth et al., 2006).

CHIMERE runs use the following input data streams: (i) meteorological fields ~~were~~ downloaded from the European Centre for Medium Range Weather Forecasts (www.ecmwf.int) at 0.5° resolution every 3 hours; (ii) anthropogenic emissions ~~were~~ aggregated at the CHIMERE resolution from the EDGARv4.3.2 database at 0.1° horizontal resolution (Crippa et al., 2016); (iii) wetland emissions ~~were~~ interpolated from the model ORCHIDEE at 0.5° horizontal resolution (Ringeval et al., 2010); (iv) boundary CH_4 concentration fields ~~were~~ extracted from the general circulation model LMDZ; these global simulations include both the chemical sinks of OH and chlorine, as well as their impact on the isotopic ratios; Cl and OH fields are prescribed offline

from the chemical model LMDZ-INCA; (v) and isotopic signatures of the different sources ~~were~~ chosen from Sherwood et al. (2017).

The chemical sink by chlorine is not included in our setup to keep simulations as light as possible. This sink can be separated into two main contributions: the upper stratosphere and the Arctic Ocean boundary layer. The upper stratosphere is not included in our model of simulation, but chlorine sink (and isotope fractionation) is expicitly accounted for in global LMDZ simulations used as boundary conditions in our setup. Regarding the Arctic Ocean boundary layer, the setup by Thonat et al. (2017) was adapted to our case, including the boundary layer Cl sink using pre-computed fields from the model LMDZ-INCA. It resulted in differences of concentrations lower than 1 ppb over the Arctic ocean, and less than 0.02‰ for the isotopic ratio of air masses, which is negligible compared to the signal we are inquiring into.

Other fluxes not included in our setup play a significant role in the regional pan-Arctic budget, such as in-land water bodies, wildfires and the sink in soil, but have limited impact on our observations. These fluxes were tested in our case and were quantified to cause differences in simulated concentrations lower than 2 ppb, and less than 0.01‰ in simulated isotopic ratios at the locations sampled during the SWERUS-C3 campaign.

2.3 Atmospheric inversion of isotopic signature

Usually observations of δ^{13}C-CH_4 are used to help constraining methane fluxes and differentiating between different sources with known signatures. However, the intrinsic spatial and temporal variability of source isotopic signatures limits the robustness of this approach (e.g., Fisher et al., 2017, as illustrated in Sect. 3.1). Here, we conversely assume that total CH_4 is properly simulated by our model (as confirmed by the good performance of the model to reproduce total CH_4 concentrations, highlighted in Sect. 3.1) and that the relative ~~contribution~~ contributions of various sources from various regions ~~is~~ are correct. Thus we use δ^{13}C-CH_4 observations to help reduce uncertainties on source isotopic signatures~~. We~~ : we test the ability of the ship-based measurements to help constrain the isotopic signature of remote sources, such as wetland sources and oceanic emissions from the Laptev, East Siberian, and Chukchi Seas, dominant in the region explored during the campaign.

To do so, δ^{13}C-CH_4 observations are implemented into a classical analytical Bayesian framework (Tarantola, 2005)~~using uncertainty and temporal correlations in signatures~~. The designed inversion system optimizes source signatures from different source types and different regions. At every time step when an isotopic observation is available, the system fits observations of isotopic ratios by altering the isotopic ratio in air masses coming from relevant source types and regions. Thus, the control vector contains one isotopic ratio value to optimize for each time step, each sector, and each region as detailed in ~~Tab. 1. The inversion system optimizes source signatures from~~ Eq. 3 below.

The isotopic ratios of wetlands, solid fossil fuels, oil and gas, other anthropogenic sources from various land regions, and a potential variety of marine sources (gas field leaks, decomposing hydrates, degrading permafrost, etc.) from the East Siberian Arctic Shelf (ESAS), as well as from air masses coming from the sides and roof of our domain of simulations are optimized in the system. Apart from ESAS, emissions are spatially differentiated into ~~24~~ 23 geographical regions (see Figure 1). Contributions from different regions and sectors are differentiated by computing so-called response functions by region, emission type and boundary side. That is to say, we carry out individual CHIMERE chemistry-transport simulations for every region, every

type of emission and every side of the domain, all the other emissions and boundary conditions being switched off, resulting in an ensemble of 98 response functions (= 23 regions × 4 sectors + ESAS + 4 sides + top).

The simulated isotopic final composition $\mathbf{y}(t)$ at every given time step t when an observation is available is retrieved by scaling relative contributions according to assumed source signatures (or original average composition for boundary conditions) . This as follows:

$$\mathbf{y}(t) = \sum_{r \in \text{regions}} \sum_{s \in \text{sectors}} \alpha_{r,s}(t) \times \delta_{r,s}(t) \tag{2}$$

with r and s varying over all available regions and sectors respectively, $\alpha^t_{r,s}$ $(0 < \alpha^t_{r,s} < 1)$ the relative contribution of the sector s from region r at time t and $\delta^t_{r,s}$ the signature in ‰ of the sector s from region r at time t.

This linear relationship allows us to define the control vector $\mathbf{x}$ and the observation operator, linking the control vector to observations of isotopic ratios, to easily compute and scale the simulated isotopic composition, but is a limiting factor as :

$$\mathbf{y}(t) = \mathbf{H}(t)\mathbf{x}(t) \text{ with } \begin{cases} \mathbf{x}(t) &= \delta_{r,s}(t) \quad \forall (r,s) \in (\text{regions}) \times (\text{sectors}) \\ \mathbf{H}(t) &= (\alpha_{r,s}(t))_{r \in \text{regions}, s \in \text{sectors}} \end{cases} \tag{3}$$

Given the prior control vector $\mathbf{x}^{\mathrm{b}}$ containing assumed source signatures before inversion, the observation vector $\mathbf{y}^{\mathrm{o}}$ and the observation operator $\mathbf{H}$, optimized signatures are obtained by solving the Bayesian problem equation:

$$\mathbf{x}^{\mathrm{a}} = \mathbf{x}^{\mathrm{b}} + \mathbf{K}(\mathbf{y}^{\mathrm{o}} - \mathbf{H}\mathbf{x}^{\mathrm{b}}) \tag{4}$$

with $\mathbf{K} = \mathbf{P}^{\mathrm{b}}\mathbf{H}^{\mathrm{T}}(\mathbf{R} + \mathbf{H}\mathbf{P}^{\mathrm{b}}\mathbf{H}^{\mathrm{T}})^{-1}$ the Kalman matrix.

The matrix $\mathbf{R}$ represents uncertainties in the observations and in the capability of the model to reproduce them. In our case, we set them uniformly to 1.5‰ (1‰ from observation errors and 0.5‰ from simulation errors). The matrix $\mathbf{P}^{\mathrm{b}}$ represents uncertainties and covariances in the prior knowledge we have on source signatures. We build the matrix $\mathbf{P}^{\mathrm{b}}$ following the values in Tab. 1, deduced from Sherwood et al. (2017) and Sapart et al. (2017). Ranges and prior signatures for boundary conditions are deduced from global simulations with the model LMDZ. Observation time steps are not optimized separately. Instead, we use temporal correlations in the $\mathbf{P}^{\mathrm{b}}$ between different time steps. We represent temporal correlations between two time steps t_i and t_j as:

$$r = exp\left(-\frac{|t_i - t_j|}{\tau}\right) \tag{5}$$

with τ the temporal correlation scale of Tab. 1.

As shown in Tab. 1, the values of source signatures are not well known and a very large range of signatures is available in the literature. To account for this large variety of realistic signatures, we carry out a Monte Carlo ensemble of 8000 inversions

Table 1. ~~Assumed isotopic~~ Isotopic signatures for the ~~different components of~~ inputs in the CHIMERE ~~forcings~~model. The min-max range is ~~centered around the~~ deduced from existing literature (Sherwood et al., 2017; Sapart et al., 2017). The prior signature ~~. Prior signatures are selected from Sherwood et al. (2017) and Sapart et al. (2017)~~is computed as the center of the min-max range.

Emission type	Prior signature (‰)	Min-Max range (‰)	Temporal correlation scale (days)
Wetlands	-65	25	~~30~~15
Fossil solid	-55	25	30
Oil & gas	-42	15	30
Other anthropogenic	-60	10	30
ESAS	-55	~~25~~ 15	~~10~~15
Boundary concentrations (sides)	-47.5	~~2~~ 0.5	~~30~~7
Boundary concentrations (top)	-47.5	~~3~~ 1	~~30~~7

with varying prior signatures and uncertainties, instead of running one single inversion. Prior signatures are sampled following a normal distribution with average and standard deviation from Tab. 1; the standard deviation is chosen as half of the min-max range. Uncertainties are sampled following a uniform distribution spanning over $[\sigma_{\text{ref}}/2, \sigma_{\text{ref}}]$, with σ_{ref} equals half of the min-max range of Tab. 1.

In the end, we obtain hourly posterior signatures for each simulated sector and region for each of the 8000 inversions. Even though posterior signatures are available for each region and each sector at each observation time step, we do not ~~account for the geographical variations of isotopic source signatures and the fact that the isotopic composition at the domain borders may vary independently from total CH_4~~ inquire into the temporal variability of sources as constraints provided by the SWERUS observations are very heterogeneous in time and space. Instead, we compute overall posterior distributions for each simulated sector and region based on an ensemble of 8000000 (=8000 inversions $\times$ 1000 hourly observations). To minimizing the impact of control vector components that are ill-constrained by the inversion, all data points are not evenly counted in posterior distributions. Posterior distributions of signatures are computed accounting for all the Monte Carlo samples and weighted by the corresponding values of the sensitivity matrix $\mathbf{KH}$ (Cardinali et al., 2004), which gives an indicator of how much observations constrain one component of the control vector. The posterior optimal signature for each region and sector is computed as the maximum of the probability distribution.

3 Results and discussion

3.1 Forward modelling of total methane and isotopic ratio

Figure 2 shows observations of total CH_4 and of isotopic ratios as measured during the campaign and compared to simulations. The model CHIMERE reproduces well most of the variability in the total CH_4 signal. The average bias over the period is lower than 5 ppb with a correlation of 0.66 between observations and simulations on an hourly basis. Most peaks spanning more than one day are properly represented in the model, proving the capability of the model to reproduce the synoptic variability of the observations. Smaller peaks are missed by the model, in particular on Aug. 5, 12 and 15, indicating that some local sources are not included in the model, or are dispersed too quickly in the numerical realm. These could be local intense seeps met along the ship~~cruise, or shore~~ 's track, or onshore wetlands not well represented with the model ORCHIDEE at 0.5° horizontal resolution. We do not investigate further missing emissions as most peaks are well explained by the model, which we assume sufficient to carry out an inversion of isotopic signatures as described in Sect. 3.2.

When computing the intersect with the y-axis of the linear fit between δ^{13}C-CH_4 and total CH_4 (see Keeling plots in Supplementary material), the observed isotope ratios point to an average generic Arctic source of $-63.0‰$, consistent with dominant biogenic sources in Arctic regions. The model reproduces well this average signature at $-59.5‰$. Observations highlight a strong synoptic variability in isotopic ratios in the Arctic, with a standard deviation of $0.50‰$ and a range of $2‰$. Most of this is missed by the model (see Fig. 2, ~~bottom panel~~top panel, prior simulation). Simulated ratios with fixed (temporally and spatially) isotopic signatures for the emission sectors detailed in Sect. 2.3 barely exhibit any variations. The prior standard deviation is $0.22‰$ (resp. $0.12‰$ when removing the wetland event on August 21st), with a range of $1.5‰$ (resp. $0.5‰$). Considering the good fit of simulations to observations of total CH_4 , the missing variability indicates that the classical assumption of uniform signatures for given sectors and regions is not valid in the Arctic, consistent with Ganesan et al. (2018) and Fisher et al. (2011). Contributions to modelled concentrations from different regions of a given emission sector can change much more than the variability of total CH_4 as indicated in Fig. 2. For instance, on July 22nd, contributions from wetlands turn from a dominating Siberian influence to a North American one, causing a change of $\sim$30 ppb in the signal. Differences in the average wetland source signatures between these two regions of $\sim 20‰$ (as suggested by Ganesan et al., 2018) would thus translate into $\sim 0.3‰$ in measured isotopic ratio, partly explaining the corresponding observed event (see middle panel of Fig. 2).

~~More~~ Still, more critical for the composition of air masses are the changes in ~~hemispheric~~ very large-scale hemispheric contributions. As indicated by the blue shades in Fig. 2 (middle panel), depending on the dominant large scale transport patterns, contributions from the stratosphere and from the model lateral sides (located in the Tropics) can vary by more than 400 ppb within a few days. This corresponds to dominantly updraught or downdraught transport patterns, as illustrated by Fig. S2 in Supplement. These very strong variations in total CH_4 enhance the impact of uncertainties in the ~~hemispheric~~ vertical and horizontal distribution of isotopic ratios at the hemispheric scale. First, tropical air masses are influenced by tropical wetlands and anthropogenic emissions, causing a spatial and temporal variability in tropical isotopic ratio of up to $1‰$, which is not accounted for in our CHIMERE ~~set-up~~ setup with fixed isotopic ratios at the simulation domain sides (see Sect.2.2). Second,

the vertical profiles of isotopic ratios in the Arctic (see simulated example from the global transport model LMDZ in Fig. S3 in Supplement) are very steep. Such gradients are poorly represented in most global models, due to issues in the representation of the vertical transport or to the insufficiently quantified fractionating OH and chlorine sinks in the stratosphere and upper troposphere. These two sources of uncertainties in chemistry-transport models coupled with the strong real-world variations in stratospheric and tropospheric contributions could explain why the ~~model~~ regional model CHIMERE does not reproduce the strong synoptic variability in δ^{13}C-CH_4 observed during the SWERUS-C3 campaign. In particular, for the above-mentioned event of July 22nd, contributions from the ~~CHIMERE domain sides ,~~ domain sides vary by more than 300 ppb. Such a variability in CH_4 contributions, associated with differences of a few ‰ between the isotopic ratios of lower stratosphere airmasses and mid/low latitude air masses, could explain the observed event.

Thus, the first order variability of atmospheric isotopic ratios is due to a balance between non-regional transport-related hemispheric features and regional contributions of wetland, ocean and anthropogenic emissions.

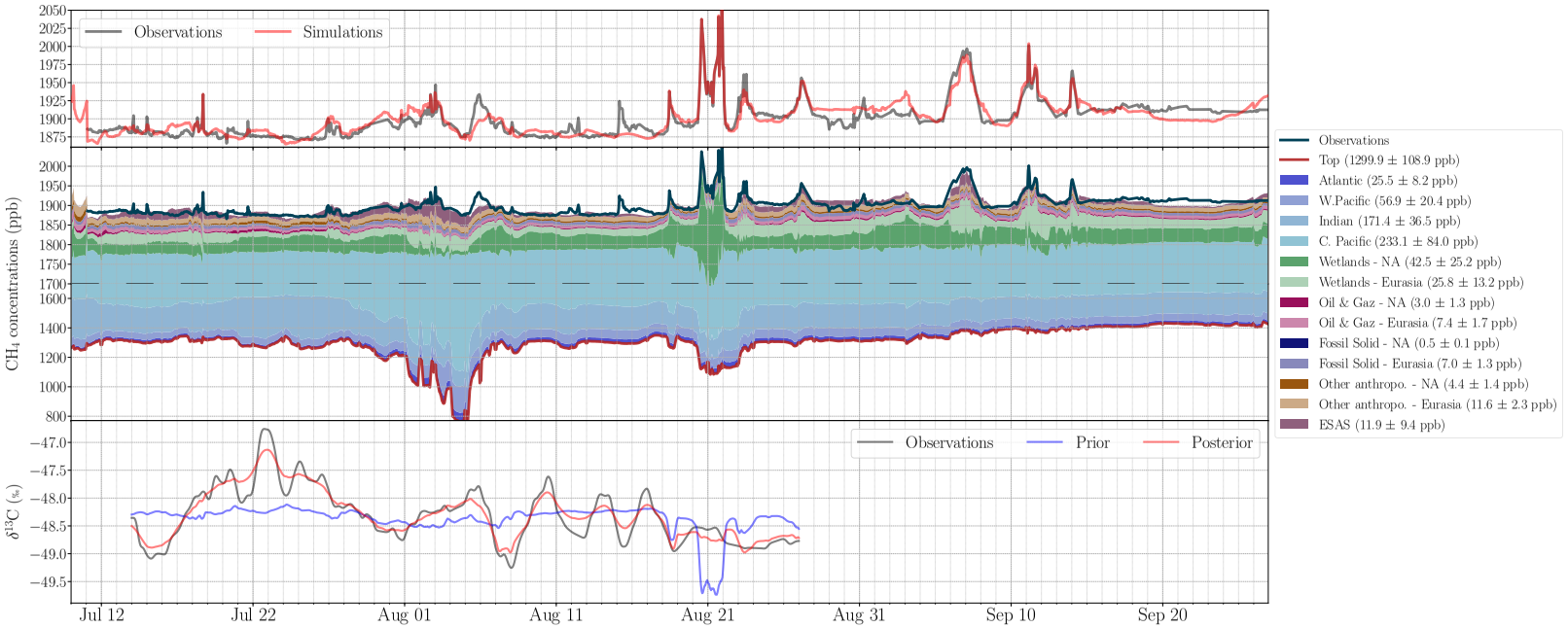

Figure 2. (top panel) Observed and simulated total CH_4 concentrations~~and~~; (middle panel) simulated contributions to total CH_4 concentrations; ~~only~~ individual regions ~~contributing more than 10 ppb on average are represented in the legend;~~ simulated by the ~~region ID and~~ model ~~side names are those of~~ (see Fig. 1) are aggregated into two main continental components: North-America (NA) and Eurasia; light green areas depict Eurasian (mostly Siberian) wetlands, while dark green ones are North American wetlands. Shaded blue areas represent contributions from the sides of the CHIMERE simulation domain (see Fig. 1); orange shades represent minor anthropogenic contribution. So-called "top" line gives the simulated concentrations originating from the lower stratosphere (i.e., from the top of CHIMERE simulation domain). Please ~~not~~ note the gap in y-axis scale at 1700 ppb ~~in~~ highlighted by the ~~middle panel~~dash line. (bottom panel) Observed and simulated isotopic ~~signatures~~ ratios before (prior) and after (posterior) inversion.

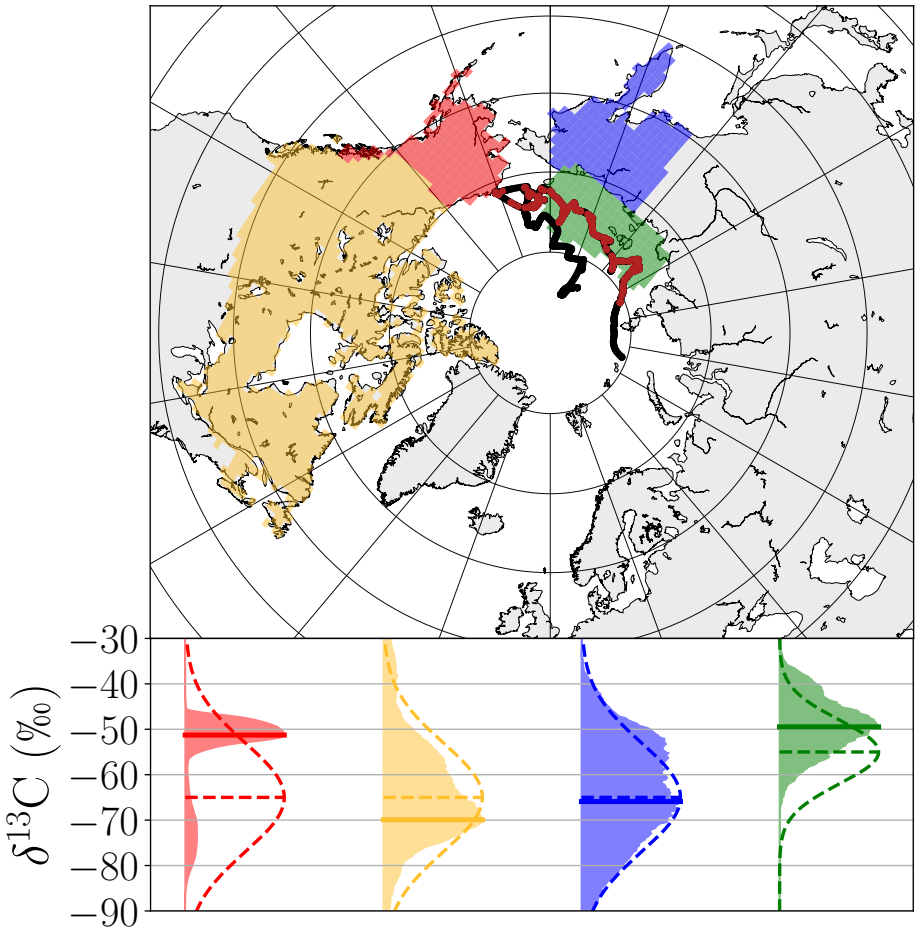

Figure 3. (top panel) Map of regions constrained by the observations ~~(~~in the inversion; for land regions, only wetlands are constrained; the green region corresponds to oceanic sources from the East Siberian Arctic Shelf; the ship path is indicated in black, with red points ~~)~~highlighting locations with available isotopes observations. (bottom panel) ~~Range~~ Distribution of posterior hourly signatures as deduced by the inversion for regions constrained by the observations for the ensemble of 8000 Monte-Carlo inversions (see details in Sect. 2.3. Prior signatures distributions (~~black crosses~~dashed lines) are those of Tab. 1. The ~~total number~~ optimal posterior signatures, defined as the maximum of ~~hours with isotopic data~~ the posterior distribution, is ~~1057.~~highlighted by plain horizontal lines.

3.2 Optimisation of Arctic source signatures

Assuming that the mix of CH_4 sources is correct, we now attempt to separate hemispheric and regional contributions by optimizing source signatures for a set of geographical regions and different emission sectors in the Arctic as detailed in Sect. 2.3. Posterior isotopic ratios in Fig. 2 (bottom panel) follow most of the variability in observations, indicating the inverse method does fit the observations in a satisfying way. The rest of the signal is within the observation uncertainties of 0.1‰. This proves

that even though the model is not perfect in representing the transport, it is reasonable to use simulated contributions to optimize isotopic signatures.

Figure 3 shows the posterior signature distributions ~~for the~~ as deduced from the 8000 Monte Carlo inversions for the four regions that are the most constrained by the observations, ~~that is to say for which the uncertainty reduction is higher than 10% per day.Only the wetland emission sector is constrained for land regions in Fig. 3. Observational constraints on the other regions are too weak according to the inversion system to be shown here. Following this definition,~~ i.e. weighted by the sensitivity matrix as detailed in Sect. 2.3. Accounting for the sensitivity matrix, it appears that only the roof boundary conditions (i.e., air masses from the lower stratosphere), ESAS emissions (i.e., emissions from the Laptev, East Siberian, and Chukchi Seas) and wetland regions on the shores of the Arctic ocean are reasonably constrained by the SWERUS-C3 ship-based campaign. Even though anthropogenic emissions were optimized in our system, only the wetland emission sector is significantly constrained for land regions (Fig. 3). The lower stratosphere signatures span in a short range of $-48.5/-46.5‰$. Wetlands are suggested to have a heavier signature in Canada (~~median: −64.0‰~~optimal signature: $-69.9‰$) than in Eastern Siberia (~~median: −54.0‰~~optimal signature: $-65.9‰$, with a node of similar importance at $-55‰$), consistent with Ganesan et al. (2018) and the compilation by Thornton et al. (2016b).

~~Fig. ?? summarizes the distributions of wetland and ESAS hourly signatures after optimization, as well a posterior signatures for airmasses coming from the lower stratosphere. The lower stratosphere signatures span in a short range of −48.5/−46.5‰. The atmospheric optimization suggests that the signatures of wetlands and ESAS span a very wide range of more than 10‰. Wetland posterior distributions have three modes in the ranges −70/−60‰, −57/−50‰ and −46/−39‰. The two first modes corresponds to wetlands in North America and Eastern Siberia respectively. The third mode is not consistent with any observed wetland signature to our knowledge; it is likely explained~~ Wetlands in Alaska exhibit a narrow posterior distribution at $-51.3‰$, with a secondary mode at $-75‰$. Alaska is thus well constrained by the inversion~~system attributing part of the signal~~. However, the final value may suggest that the inversion has difficulties in differentiating collocated emissions and mixes the signal due to thermogenic sources ~~co-located with~~ with co-located wetland emissions, as it is the case in ~~both Siberia and Canada~~ Alaska with extensive extraction of raw oil and gas.

Posterior ESAS signatures are ~~mostly distributed in the range -48/-40‰ (median: −43.7‰), with a secondary mode in the range -50/-58~~significantly shifted by more than 5‰ to $-49.5‰$ from the prior signature towards lighter values. This compares with previous studies and points towards a mix of different processes taking place in the Arctic shelf such as inputs from the sea bed ~~(James et al., 2016; Berchet et al., 2016; Skorokhod et al., 2016; Pankratova et al., 2018). The lighter mode is dominated by thermogenic sources while the heavier mode could~~ (James et al., 2016; Berchet et al., 2016; Skorokhod et al., 2016; Pankratova et al., 20 . The posterior signature could thus be explained by mixed biogenic and thermogenic sources, confirming that ESAS emissions, possibly including an hydrate contribution, are not as depleted as wetland sources (Cramer et al., 1999; Lorenson, 1999).

Overall, the approach developed here reveals that the spatial and temporal variations of isotopic source signatures must be accounted for in order to properly represent δ^{13}C-CH_4 observations. Such an approach does not allow us to reach definitive conclusions when considering the spread of the inferred regional isotopic signatures. However, it is crucial to account for isotopic ratios to avoid misallocating methane flux variations in methane inversions. We also show that atmospheric δ^{13}C-CH_4

signals can be significant (larger than observation errors), indicating a good potential for the use of isotopic observations based on oceanic campaign to improve our knowledge of the Arctic methane cycle. Finally, the weight of the boundary conditions in the signal points at necessary progress in global simulations (including fractionating chemical reactions in the stratosphere) of CH_4 atmospheric isotopic ratios.

4 Conclusions

Observations of total atmospheric methane and isotopic ratio were carried out in Summer 2014 in the Arctic Ocean during the SWERUS-C3 campaign onboard the Swedish icebreaker *Oden*. A unique continuous dataset of 45 days of ~~isotopic ratio in~~ atmospheric isotopic ratios over the Arctic Ocean is available from this campaign. Consistently with other campaigns in the region collecting flasks, the synoptic variability of atmospheric isotopic ratios in the Arctic is very strong, spanning $\sim 2‰$, largely above observation error. Using forward simulations, we confirmed that the assumption of uniform isotopic ~~signature~~ signatures to represent emission sectors is invalid in the Arctic dominated by natural sources. We also exhibited the strong dependency of atmospheric isotopic ratios to large-scale changes in air mass origin (lateral boundaries of our simulation domain, corresponding to mid-/low-latitude air masses; top boundaries corresponding to lower stratosphere air masses). Based on a simplified inversion framework, the SWERUS-C3 data were used to infer isotopic source signatures of the Arctic regions and emission sectors. Due to the limited number of available observations and the important distance between sources and observations, our system was not able to provide any significant constraints on anthropogenic emissions, and could optimize signatures from ESAS and wetlands near the Arctic Ocean shores only. Wetland and oceanic ESAS source signatures were found to span a very wide range with a multimodal distribution for ~~ESAS~~wetlands. The inversion also indicated that CH_4 emissions from ESAS are composed of a mixture of dominant thermogenic methane, complemented by some biogenic methane.

Overall, only a strong spatial and temporal variability in emission signatures and in stratospheric isotopic ratios can explain the variability of observations. Therefore, our study points at necessary improvements in simulating the first-order transport and chemistry of methane and its isotopes to reproduce large scale hemispheric features, especially stratosphere to troposphere exchanges. This makes it necessary to improve i) the quality of continuous isotopic measurements to capture the synoptic signal with even higher confidence, ii) numerical chemistry-transport models, so that the uncertainties on the first-order processes are at least one order of magnitude smaller than the regional signal, which is not the case ~~today~~in our study, and iii) the mapping of isotopic emission signatures used as ~~prior~~ priors in inversions as initiated by Ganesan et al. (2018).

Author ~~contribution~~contributions

AB, TT and IP designed the simulation experiments. AB and TT developed the code and performed the CHIMERE numerical simulations. TH and JT ~~run~~ ran global simulations. PC and BT designed, carried out and provided observation data from the SWERUS-C3 campaign. PB, MS and JDP contributed to the scientific analysis of this work. AB prepared the manuscript with ~~contribution from all~~ contributions from co-authors.

Code/Data availability

The isotopic ratio and total CH_4 observation data are available upon request. The transport model CHIMERE can be downloaded here: https://www.lmd.polytechnique.fr/chimere/. CHIMERE simulations were driven by the inversion system PYVAR-CHIMERE (Fortems-Cheiney et al., 2019). Inputs for our CHIMERE simulations are freely available following instructions detailed in respective references in Sect. 2.2.

Competing interests

The authors declare no competing interests.

Acknowledgements. We thank the crew of I/B *Oden* who made the SWERUS-C3 expedition possible. SWERUS-C3 funding was provided by the Knut and Alice Wallenberg Foundation, Vetenskapsrådet (Swedish Research Council), Stockholm University, Swedish Polar Research Secretariat, and the Bolin Centre for Climate Research. δ^{13}C-CH_4 observations from SWERUS-C3 campaign will be posted to the Bolin Centre database, https://bolin.su.se/data/. This work has been supported by the Swedish Research Council VR through a Franco-Swedish project named IZOMET-FS "Distinguishing Arctic CH_4 sources to the atmosphere using inverse analysis of high-frequency CH_4 , δ^{13}C-CH_4 and CH_3D measurements" ~~project~~(grant no. VR 2014-6584). The study extensively relies on the meteorological data provided by the ECMWF. Calculations were performed using the computing resources of LSCE, maintained by François Marabelle and the LSCE IT team.

References

Arora, V. K., Berntsen, T., Biastock, A., Bousquet, P., Bruhwiler, L., Bush, E., Chan, E., Christensen, T. R., Dlugokencky, E., Fisher, R. E., France, J., Gauss, M., H\"oglund-Isaksson, L., Houweling, S., Huissteden, K., and Janssens-Maenhout, G.: AMAP, 2015. AMAP Assessment 2015: Methane as an Arctic climate forcer, Tech. rep., Arctic Monitoring and Assessment Programme (AMAP), Oslo, Norway, https://www.amap.no/documents/doc/amap-assessment-2015-methane-as-an-arctic-climate-forcer/1285, 2015.

Arshinov, M. Y., Belan, B. D., Davydov, D. K., Inouye, G., Krasnov, O. A., Maksyutov, S., Machida, T., Fofonov, A. V., and Shimoyama, K.: Spatial and temporal variability of CO$_2$ and CH$_4$ concentrations in the surface atmospheric layer over West Siberia, Atmos Ocean Opt, 22, 84–93, https://doi.org/10.1134/S1024856009010126, http://link.springer.com/article/10.1134/S1024856009010126, 2009.

Berchet, A., Pison, I., Chevallier, F., Paris, J.-D., Bousquet, P., Bonne, J.-L., Arshinov, M. Y., Belan, B. D., Cressot, C., Davydov, D. K., Dlugokencky, E. J., Fofonov, A. V., Galanin, A., Lavrič, J., Machida, T., Parker, R., Sasakawa, M., Spahni, R., Stocker, B. D., and Winderlich, J.: Natural and anthropogenic methane fluxes in Eurasia: a mesoscale quantification by generalized atmospheric inversion, Biogeosciences, 12, 5393–5414, https://doi.org/https://doi.org/10.5194/bg-12-5393-2015, https://www.biogeosciences.net/12/5393/2015/bg-12-5393-2015.html, 2015.

Berchet, A., Bousquet, P., Pison, I., Locatelli, R., Chevallier, F., Paris, J.-D., Dlugokencky, E. J., Laurila, T., Hatakka, J., Viisanen, Y., Worthy, D. E. J., Nisbet, E., Fisher, R., France, J., Lowry, D., Ivakhov, V., and Hermansen, O.: Atmospheric constraints on the methane emissions from the East Siberian Shelf, Atmos. Chem. Phys., 16, 4147–4157, https://doi.org/10.5194/acp-16-4147-2016, http://www.atmos-chem-phys.net/16/4147/2016/, 2016.

Bohn, T. J., Melton, J. R., Ito, A., Kleinen, T., Spahni, R., Stocker, B. D., Zhang, B., Zhu, X., Schroeder, R., Glagolev, M. V., Maksyutov, S., Brovkin, V., Chen, G., Denisov, S. N., Eliseev, A. V., Gallego-Sala, A., McDonald, K. C., Rawlins, M., Riley, W. J., Subin, Z. M., Tian, H., Zhuang, Q., and Kaplan, J. O.: WETCHIMP-WSL: intercomparison of wetland methane emissions models over West Siberia, Biogeosciences, 12, 3321–3349, https://doi.org/10.5194/bg-12-3321-2015, http://www.biogeosciences.net/12/3321/2015/, 2015.

Cardinali, C., Pezzulli, S., and Andersson, E.: Influence-matrix diagnostic of a data assimilation system, Q. J. R. Meteorol. Soc., 130, 2767–2786, https://doi.org/10.1256/qj.03.205, http://onlinelibrary.wiley.com/doi/10.1256/qj.03.205/abstract, 2004.

Charkin, A. N., Dudarev, O. V., Semiletov, I. P., Kruhmalev, A. V., Vonk, J. E., S\‘anchez-Garc\’ia, L., Karlsson, E., and Gustafsson, \.: Seasonal and interannual variability of sedimentation and organic matter distribution in the Buor-Khaya Gulf: the primary recipient of input from Lena River and coastal erosion in the southeast Laptev Sea, Biogeosciences, 8, 2581–2594, https://doi.org/https://doi.org/10.5194/bg-8-2581-2011, https://www.biogeosciences.net/8/2581/2011/bg-8-2581-2011.html, 2011.

Craig, H.: Isotopic standards for carbon and oxygen and correction factors for mass-spectrometric analysis of carbon dioxide, Geochimica et Cosmochimica Acta, 12, 133–149, https://doi.org/10.1016/0016-7037(57)90024-8, http://www.sciencedirect.com/science/article/pii/0016703757900248, 1957.

Cramer, B., Poelchau, H. S., Gerling, P., Lopatin, N. V., and Littke, R.: Methane released from groundwater: the source of natural gas accumulations in northern West Siberia, Marine and Petroleum Geology, 16, 225–244, https://doi.org/10.1016/S0264-8172(98)00085-3, http://www.sciencedirect.com/science/article/pii/S0264817298000853, 1999.

Crippa, M., Janssens-Maenhout, G., Dentener, F., Guizzardi, D., Sindelarova, K., Muntean, M., Van Dingenen, R., and Granier, C.: Forty years of improvements in European air quality: regional policy-industry interactions with global impacts, Atmospheric Chemistry and Physics, 16, 3825–3841, https://doi.org/https://doi.org/10.5194/acp-16-3825-2016, https://www.atmos-chem-phys.net/16/3825/2016/, 2016.

Dlugokencky, E. J., Bruhwiler, L., White, J. W. C., Emmons, L. K., Novelli, P. C., Montzka, S. A., Masarie, K. A., Lang, P. M., Crotwell, A. M., Miller, J. B., and Gatti, L. V.: Observational constraints on recent increases in the atmospheric CH$_4$ burden, Geophys. Res. Lett., 36, L18 803, https://doi.org/10.1029/2009GL039780, http://onlinelibrary.wiley.com/doi/10.1029/2009GL039780/abstract, 2009.

Dlugokencky, E. J., Crotwell, A. M., Lang, P. M., and Masarie, K. A.: Atmospheric methane dry air mole Fractions from quasi-continuous measurements at Barrow, Alaska and Mauna Loa, Hawaii, 1986-2013, ftp://ftp.cmdl.noaa.gov/ccg/ch4/in-situ/, 2014.

Dmitrenko, I. A., Kirillov, S. A., Tremblay, L. B., Kassens, H., Anisimov, O. A., Lavrov, S. A., Razumov, S. O., and Grigoriev, M. N.: Recent changes in shelf hydrography in the Siberian Arctic: Potential for subsea permafrost instability, Journal of Geophysical Research: Oceans, 116, https://doi.org/10.1029/2011JC007218, https://agupubs.onlinelibrary.wiley.com/doi/10.1029/2011JC007218, 2011.

Fisher, R. E., Sriskantharajah, S., Lowry, D., Lanoisellé, M., Fowler, C. M. R., James, R. H., Hermansen, O., Lund Myhre, C., Stohl, A., Greinert, J., Nisbet-Jones, P. B. R., Mienert, J., and Nisbet, E. G.: Arctic methane sources: Isotopic evidence for atmospheric inputs, Geophys. Res. Lett., 38, L21 803, https://doi.org/10.1029/2011GL049319, http://onlinelibrary.wiley.com/doi/10.1029/2011GL049319/abstract, 2011.

Fisher, R. E., France, J. L., Lowry, D., Lanoisellé, M., Brownlow, R., Pyle, J. A., Cain, M., Warwick, N., Skiba, U. M., Drewer, J., Dinsmore, K. J., Leeson, S. R., Bauguitte, S. J.-B., Wellpott, A., O'Shea, S. J., Allen, G., Gallagher, M. W., Pitt, J., Percival, C. J., Bower, K., George, C., Hayman, G. D., Aalto, T., Lohila, A., Aurela, M., Laurila, T., Crill, P. M., McCalley, C. K., and Nisbet, E. G.: Measurement of the 13C isotopic signature of methane emissions from northern European wetlands, Global Biogeochemical Cycles, 31, 605–623, https://doi.org/10.1002/2016GB005504, https://agupubs.onlinelibrary.wiley.com/doi/abs/10.1002/2016GB005504, 2017.

Folberth, G. A., Hauglustaine, D. A., Lathière, J., and Brocheton, F.: Interactive chemistry in the Laboratoire de Météorologie Dynamique general circulation model: model description and impact analysis of biogenic hydrocarbons on tropospheric chemistry, Atmospheric Chemistry and Physics, 6, 2273–2319, https://doi.org/https://doi.org/10.5194/acp-6-2273-2006, https://www.atmos-chem-phys.net/6/2273/2006/, 2006.

Fortems-Cheiney, A., Pison, I., Dufour, G., Broquet, G., Berchet, A., Potier, E., Coman, A., Siour, G., and Costantino, L.: Variational regional inverse modeling of reactive species emissions with PYVAR-CHIMERE, Geoscientific Model Development Discussions, pp. 1–22, https://doi.org/https://doi.org/10.5194/gmd-2019-186, https://www.geosci-model-dev-discuss.net/gmd-2019-186/, 2019.

Ganesan, A. L., Stell, A. C., Gedney, N., Comyn-Platt, E., Hayman, G., Rigby, M., Poulter, B., and Hornibrook, E. R. C.: Spatially Resolved Isotopic Source Signatures of Wetland Methane Emissions, Geophysical Research Letters, 45, 3737–3745, https://doi.org/10.1002/2018GL077536, https://agupubs.onlinelibrary.wiley.com/doi/abs/10.1002/2018GL077536, 2018.

Hauglustaine, D. A., Hourdin, F., Jourdain, L., Filiberti, M.-A., Walters, S., Lamarque, J.-F., and Holland, E. A.: Interactive chemistry in the Laboratoire de Météorologie Dynamique general circulation model: Description and background tropospheric chemistry evaluation, Journal of Geophysical Research: Atmospheres, 109, https://doi.org/10.1029/2003JD003957, https://agupubs.onlinelibrary.wiley.com/doi/abs/10.1029/2003JD003957, 2004.

Ishizawa, M., Chan, D., Worthy, D., Chan, E., Vogel, F., and Maksyutov, S.: Analysis of atmospheric CH_4 in Canadian Arctic and estimation of the regional CH_4 fluxes, Atmospheric Chemistry and Physics, 19, 4637–4658, https://doi.org/https://doi.org/10.5194/acp-19-4637-2019, https://www.atmos-chem-phys.net/19/4637/2019/, 2019.

James, R. H., Bousquet, P., Bussmann, I., Haeckel, M., Kipfer, R., Leifer, I., Niemann, H., Ostrovsky, I., Piskozub, J., Rehder, G., Treude, T., Vielstädte, L., and Greinert, J.: Effects of climate change on methane emissions from seafloor sediments in the Arctic Ocean: A review, Limnology and Oceanography, 61, S283–S299, https://doi.org/10.1002/lno.10307, https://aslopubs.onlinelibrary.wiley.com/doi/abs/10.1002/lno.10307, 2016.

Kirschke, S., Bousquet, P., Ciais, P., Saunois, M., Canadell, J. G., Dlugokencky, E. J., Bergamaschi, P., Bergmann, D., Blake, D. R., Bruhwiler, L., Cameron-Smith, P., Castaldi, S., Chevallier, F., Feng, L., Fraser, A., Heimann, M., Hodson, E. L., Houweling, S., Josse, B., Fraser, P. J., Krummel, P. B., Lamarque, J.-F., Langenfelds, R. L., Le Quéré, C., Naik, V., O'Doherty, S., Palmer, P. I., Pison, I., Plummer, D., Poulter, B., Prinn, R. G., Rigby, M., Ringeval, B., Santini, M., Schmidt, M., Shindell, D. T., Simpson, I. J., Spahni, R., Steele, L. P., Strode, S. A., Sudo, K., Szopa, S., van der Werf, G. R., Voulgarakis, A., van Weele, M., Weiss, R. F., Williams, J. E., and Zeng, G.: Three decades of global methane sources and sinks, Nature Geosci, 6, 813–823, https://doi.org/10.1038/ngeo1955, http://www.nature.com/ngeo/journal/v6/n10/full/ngeo1955.html, 2013.

Lorenson, T.: Gas composition and isotopic geochemistry of cuttings, core, and gas hydrate from the JAPEX/JNOC/GSC Mallik 2L-38 gas hydrate research well, Bulletin of the Geological Survey of Canada, p. 21, http://pubs.er.usgs.gov/publication/70021662, 1999.

McCalley, C. K., Woodcroft, B. J., Hodgkins, S. B., Wehr, R. A., Kim, E.-H., Mondav, R., Crill, P. M., Chanton, J. P., Rich, V. I., Tyson, G. W., and Saleska, S. R.: Methane dynamics regulated by microbial community response to permafrost thaw, Nature, 514, 478–481, https://doi.org/10.1038/nature13798, https://www.nature.com/articles/nature13798, 2014.

McGuire, A. D., Anderson, L. G., Christensen, T. R., Dallimore, S., Guo, L., Hayes, D. J., Heimann, M., Lorenson, T. D., Macdonald, R. W., and Roulet, N.: Sensitivity of the carbon cycle in the Arctic to climate change, Ecological Monographs, 79, 523–555, https://doi.org/10.1890/08-2025.1, http://www.esajournals.org/doi/abs/10.1890/08-2025.1, 2009.

Menut, L., Bessagnet, B., Khvorostyanov, D., Beekmann, M., Blond, N., Colette, A., Coll, I., Curci, G., Foret, G., Hodzic, A., Mailler, S., Meleux, F., Monge, J.-L., Pison, I., Siour, G., Turquety, S., Valari, M., Vautard, R., and Vivanco, M. G.: CHIMERE 2013: a model for regional atmospheric composition modelling, Geosci. Model Dev., 6, 981–1028, https://doi.org/10.5194/gmd-6-981-2013, http://www.geosci-model-dev.net/6/981/2013/, 2013.

Nisbet, E. G., Dlugokencky, E. J., Manning, M. R., Lowry, D., Fisher, R. E., France, J. L., Michel, S. E., Miller, J. B., White, J. W. C., Vaughn, B., Bousquet, P., Pyle, J. A., Warwick, N. J., Cain, M., Brownlow, R., Zazzeri, G., Lanoisellé, M., Manning, A. C., Gloor, E., Worthy, D. E. J., Brunke, E.-G., Labuschagne, C., Wolff, E. W., and Ganesan, A. L.: Rising atmospheric methane: 2007–2014 growth and isotopic shift, Global Biogeochemical Cycles, 30, 1356–1370, https://doi.org/10.1002/2016GB005406, https://agupubs.onlinelibrary.wiley.com/doi/abs/10.1002/2016GB005406, 2016.

Nisbet, E. G., Manning, M. R., Dlugokencky, E. J., Fisher, R. E., Lowry, D., Michel, S. E., Myhre, C. L., Platt, S. M., Allen, G., Bousquet, P., Brownlow, R., Cain, M., France, J. L., Hermansen, O., Hossaini, R., Jones, A. E., Levin, I., Manning, A. C., Myhre, G., Pyle, J. A., Vaughn, B. H., Warwick, N. J., and White, J. W. C.: Very Strong Atmospheric Methane Growth in the 4 Years 2014–2017: Implications for the Paris Agreement, Global Biogeochemical Cycles, 33, 318–342, https://doi.org/10.1029/2018GB006009, https://agupubs.onlinelibrary.wiley.com/doi/abs/10.1029/2018GB006009, 2019.

Pankratova, N., Skorokhod, A., Belikov, I., Elansky, N., Rakitin, V., Shtabkin, Y., and Berezina, E.: EVIDENCE OF ATMOSPHERIC RESPONSE TO METHANE EMISSIONS FROM THE EAST SIBERIAN ARCTIC SHELF, https://ges.rgo.ru/jour/article/view/383, 2018.

Pankratova, N., Belikov, I., Skorokhod, A., Belousov, V., Artamonov, A., Repina, I., and Shishov, E.: Measurements and data processing of atmospheric CO$_2$, CH$_4$, H$_2$O and δ^{13}C-CH$_4$ mixing ratio during the ship campaign in the East Arctic and the Far East seas in autumn 2016, IOP Conf. Ser.: Earth Environ. Sci., 231, 012 041, https://doi.org/10.1088/1755-1315/231/1/012041, https://doi.org/10.1088%2F1755-1315%2F231%2F1%2F012041, 2019.

Paris, J. D., Ciais, P., Nédélec, P., Stohl, A., Belan, B. D., Arshinov, M. Y., Carouge, C., Golitsyn, G. S., and Granberg, I. G.: New insights on the chemical composition of the Siberian air shed from the YAK-AEROSIB aircraft campaigns, B. Am. Meteorol. Soc., 91, 625–641, http://zardoz.nilu.no/~andreas/publications/168.pdf, 2010.

Pisso, I., Myhre, C. L., Platt, S. M., Eckhardt, S., Hermansen, O., Schmidbauer, N., Mienert, J., Vadakkepuliyambatta, S., Bauguitte, S., Pitt, J., Allen, G., Bower, K. N., O'Shea, S., Gallagher, M. W., Percival, C. J., Pyle, J., Cain, M., and Stohl, A.: Constraints on oceanic methane emissions west of Svalbard from atmospheric in situ measurements and Lagrangian transport modeling, J. Geophys. Res. Atmos., 121, 2016JD025 590, https://doi.org/10.1002/2016JD025590, http://onlinelibrary.wiley.com/doi/10.1002/2016JD025590/abstract, 2016.

Ringeval, B., de Noblet-Ducoudré, N., Ciais, P., Bousquet, P., Prigent, C., Papa, F., and Rossow, W. B.: An attempt to quantify the impact of changes in wetland extent on methane emissions on the seasonal and interannual time scales, Global Biogeochemical Cycles, 24, https://doi.org/10.1029/2008GB003354, http://onlinelibrary.wiley.com.biblioplanets.gate.inist.fr/doi/10.1029/2008GB003354/abstract, 2010.

Ruppel, C. D. and Kessler, J. D.: The interaction of climate change and methane hydrates, Reviews of Geophysics, 55, 126–168, https://doi.org/10.1002/2016RG000534, https://agupubs.onlinelibrary.wiley.com/doi/10.1002/2016RG000534, 2017.

Sapart, C. J., Shakhova, N., Semiletov, I., Jansen, J., Szidat, S., Kosmach, D., Dudarev, O., Veen, C. v. d., Egger, M., Sergienko, V., Salyuk, A., Tumskoy, V., Tison, J.-L., and Röckmann, T.: The origin of methane in the East Siberian Arctic Shelf unraveled with triple isotope analysis, Biogeosciences, 14, 2283–2292, https://doi.org/https://doi.org/10.5194/bg-14-2283-2017, https://www.biogeosciences.net/14/2283/2017/, 2017.

Sasakawa, M., Shimoyama, K., Machida, T., Tsuda, N., Suto, H., Arshinov, M., Davydov, D., Fofonov, A., Krasnov, O., Saeki, T., Koyama, Y., and Maksyutov, S.: Continuous measurements of methane from a tower network over Siberia, Tellus B, 62, 403–416, https://doi.org/10.1111/j.1600-0889.2010.00494.x, http://onlinelibrary.wiley.com/doi/10.1111/j.1600-0889.2010.00494.x/abstract, 2010.

Saunois, M., Bousquet, P., Poulter, B., Peregon, A., Ciais, P., Canadell, J. G., Dlugokencky, E. J., Etiope, G., Bastviken, D., Houweling, S., Janssens-Maenhout, G., Tubiello, F. N., Castaldi, S., Jackson, R. B., Alexe, M., Arora, V. K., Beerling, D. J., Bergamaschi, P., Blake, D. R., Brailsford, G., Brovkin, V., Bruhwiler, L., Crevoisier, C., Crill, P., Covey, K., Curry, C., Frankenberg, C., Gedney, N., Höglund-Isaksson, L., Ishizawa, M., Ito, A., Joos, F., Kim, H.-S., Kleinen, T., Krummel, P., Lamarque, J.-F., Langenfelds, R., Locatelli, R., Machida, T., Maksyutov, S., McDonald, K. C., Marshall, J., Melton, J. R., Morino, I., Naik, V., O'Doherty, S., Parmentier, F.-J. W., Patra, P. K., Peng, C., Peng, S., Peters, G. P., Pison, I., Prigent, C., Prinn, R., Ramonet, M., Riley, W. J., Saito, M., Santini, M., Schroeder, R., Simpson, I. J., Spahni, R., Steele, P., Takizawa, A., Thornton, B. F., Tian, H., Tohjima, Y., Viovy, N., Voulgarakis, A., Weele, M. v., Werf, G. R. v. d., Weiss, R., Wiedinmyer, C., Wilton, D. J., Wiltshire, A., Worthy, D., Wunch, D., Xu, X., Yoshida, Y., Zhang, B., Zhang, Z., and Zhu, Q.: The global methane budget 2000–2012, Earth System Science Data, 8, 697–751, https://doi.org/https://doi.org/10.5194/essd-8-697-2016, https://www.earth-syst-sci-data.net/8/697/2016/, 2016.

Saunois, M., Bousquet, P., Poulter, B., Peregon, A., Ciais, P., Canadell, J. G., Dlugokencky, E. J., Etiope, G., Bastviken, D., Houweling, S., Janssens-Maenhout, G., Tubiello, F. N., Castaldi, S., Jackson, R. B., Alexe, M., Arora, V. K., Beerling, D. J., Bergamaschi, P., Blake, D. R., Brailsford, G., Bruhwiler, L., Crevoisier, C., Crill, P., Covey, K., Frankenberg, C., Gedney, N., Höglund-Isaksson, L., Ishizawa, M., Ito, A., Joos, F., Kim, H.-S., Kleinen, T., Krummel, P., Lamarque, J.-F., Langenfelds, R., Locatelli, R., Machida, T., Maksyutov, S., Melton, J. R., Morino, I., Naik, V., O'Doherty, S., Parmentier, F.-J. W., Patra, P. K., Peng, C., Peng, S., Peters, G. P., Pison, I., Prinn, R., Ramonet, M., Riley, W. J., Saito, M., Santini, M., Schroeder, R., Simpson, I. J., Spahni, R., Takizawa, A., Thornton, B. F., Tian, H., Tohjima, Y., Viovy, N., Voulgarakis, A., Weiss, R., Wilton, D. J., Wiltshire, A., Worthy, D., Wunch, D., Xu, X., Yoshida, Y., Zhang, B., Zhang, Z., and

Zhu, Q.: Variability and quasi-decadal changes in the methane budget over the period 2000–2012, Atmospheric Chemistry and Physics, 17, 11 135–11 161, https://doi.org/https://doi.org/10.5194/acp-17-11135-2017, https://www.atmos-chem-phys.net/17/11135/2017/, 2017.

Shakhova, N., Semiletov, I., Salyuk, A., Yusupov, V., Kosmach, D., and Gustafsson, O.: Extensive Methane Venting to the Atmosphere from Sediments of the East Siberian Arctic Shelf, Science, 327, 1246–1250, https://doi.org/10.1126/science.1182221, http://www.sciencemag.org/content/327/5970/1246, 2010.

Shakhova, N., Semiletov, I., Leifer, I., Sergienko, V., Salyuk, A., Kosmach, D., Chernykh, D., Stubbs, C., Nicolsky, D., Tumskoy, V., and Gustafsson, \.: Ebullition and storm-induced methane release from the East Siberian Arctic Shelf, Nature Geosci, 7, 64–70, https://doi.org/10.1038/ngeo2007, http://www.nature.com/ngeo/journal/v7/n1/abs/ngeo2007.html, 2014.

Sherwood, O. A., Schwietzke, S., Arling, V. A., and Etiope, G.: Global Inventory of Gas Geochemistry Data from Fossil Fuel, Microbial and Burning Sources, version 2017, Earth System Science Data, 9, 639–656, https://doi.org/https://doi.org/10.5194/essd-9-639-2017, https://www.earth-syst-sci-data.net/9/639/2017/, 2017.

Skorokhod, A. I., Pankratova, N. V., Belikov, I. B., Thompson, R. L., Novigatsky, A. N., and Golitsyn, G. S.: Observations of atmospheric methane and its stable isotope ratio (δ^{13}C) over the Russian Arctic seas from ship cruises in the summer and autumn of 2015, Dokl. Earth Sc., 470, 1081–1085, https://doi.org/10.1134/S1028334X16100160, https://doi.org/10.1134/S1028334X16100160, 2016.

Tan, Z., Zhuang, Q., Henze, D. K., Frankenberg, C., Dlugokencky, E., Sweeney, C., Turner, A. J., Sasakawa, M., and Machida, T.: Inverse modeling of pan-Arctic methane emissions at high spatial resolution: what can we learn from assimilating satellite retrievals and using different process-based wetland and lake biogeochemical models?, Atmospheric Chemistry and Physics, 16, 12 649–12 666, https://doi.org/https://doi.org/10.5194/acp-16-12649-2016, https://www.atmos-chem-phys.net/16/12649/2016/, 2016.

Tarantola, A.: Inverse problem theory and methods for model parameter estimation: SIAM, Society for Industrial and Applied Mathematics, 3600, 19 104–2688, 2005.

Tarasova, O., Brenninkmeijer, C., Assonov, S., Elansky, N., Röckmann, T., and Brass, M.: Atmospheric CH$_4$ along the Trans-Siberian railroad (TROICA) and river Ob: Source identification using stable isotope analysis, Atmospheric Environment, 40, 5617–5628, https://doi.org/10.1016/j.atmosenv.2006.04.065, http://www.sciencedirect.com/science/article/pii/S1352231006004614, 2006.

Tarasova, O. A., Houweling, S., Elansky, N., and Brenninkmeijer, C. A. M.: Application of stable isotope analysis for improved understanding of the methane budget: comparison of TROICA measurements with TM3 model simulations, J Atmos Chem, 63, 49–71, https://doi.org/10.1007/s10874-010-9157-y, http://link.springer.com/article/10.1007/s10874-010-9157-y, 2009.

Thompson, R. L., Sasakawa, M., Machida, T., Aalto, T., Worthy, D., Lavric, J. V., Lund Myhre, C., and Stohl, A.: Methane fluxes in the high northern latitudes for 2005–2013 estimated using a Bayesian atmospheric inversion, Atmos. Chem. Phys., 17, 3553–3572, https://doi.org/10.5194/acp-17-3553-2017, http://www.atmos-chem-phys.net/17/3553/2017/, 2017.

Thonat, T., Saunois, M., Bousquet, P., Pison, I., Tan, Z., Zhuang, Q., Crill, P. M., Thornton, B. F., Bastviken, D., Dlugokencky, E. J., Zimov, N., Laurila, T., Hatakka, J., Hermansen, O., and Worthy, D. E. J.: Detectability of Arctic methane sources at six sites performing continuous atmospheric measurements, Atmos. Chem. Phys., 17, 8371–8394, https://doi.org/10.5194/acp-17-8371-2017, https://www.atmos-chem-phys.net/17/8371/2017/, 2017.

Thornton, B. F., Geibel, M. C., Crill, P. M., Humborg, C., and Mörth, C.-M.: Methane fluxes from the sea to the atmosphere across the Siberian shelf seas, Geophys. Res. Lett., 43, 2016GL068 977, https://doi.org/10.1002/2016GL068977, http://onlinelibrary.wiley.com/doi/10.1002/2016GL068977/abstract, 2016a.

Thornton, B. F., Wik, M., and Crill, P. M.: Double-counting challenges the accuracy of high-latitude methane inventories, Geophys. Res. Lett., p. 2016GL071772, https://doi.org/10.1002/2016GL071772, http://onlinelibrary.wiley.com/doi/10.1002/2016GL071772/abstract, 2016b.

Thornton, B. F., Prytherch, J., Andersson, K., Brooks, I. M., Salisbury, D., Tjernström, M., and Crill, P. M.: Shipborne eddy covariance observations of methane fluxes constrain Arctic sea emissions, Science Advances, 6, eaay7934, https://doi.org/10.1126/sciadv.aay7934, https://advances.sciencemag.org/content/6/5/eaay7934, 2020.

Turner, A. J., Frankenberg, C., and Kort, E. A.: Interpreting contemporary trends in atmospheric methane, PNAS, 116, 2805–2813, https://doi.org/10.1073/pnas.1814297116, https://www.pnas.org/content/116/8/2805, 2019.

Warwick, N. J., Cain, M. L., Fisher, R., France, J. L., Lowry, D., Michel, S. E., Nisbet, E. G., Vaughn, B. H., White, J. W. C., and Pyle, J. A.: Using $delta^{13}$C-CH$_4$ and δD-CH$_4$ to constrain Arctic methane emissions, Atmos. Chem. Phys., 16, 14 891–14 908, https://doi.org/10.5194/acp-16-14891-2016, http://www.atmos-chem-phys.net/16/14891/2016/, 2016.

Xiong, X., Barnet, C., Maddy, E., Sweeney, C., Liu, X., Zhou, L., and Goldberg, M.: Characterization and validation of methane products from the Atmospheric Infrared Sounder (AIRS), Journal of Geophysical Research: Biogeosciences, 113, https://doi.org/10.1029/2007JG000500, https://agupubs.onlinelibrary.wiley.com/doi/full/10.1029/2007JG000500, 2008.

Yu, J., Xie, Z., Sun, L., Kang, H., He, P., and Xing, G.: δ^{13}C-CH4 reveals CH4 variations over oceans from mid-latitudes to the Arctic, Scientific Reports, 5, 13 760, https://doi.org/10.1038/srep13760, https://www.nature.com/articles/srep13760, 2015.